ACS APPLIED NANO MATERIALS

www.acsanm.org

Review

Extending the Optical Absorption Limit of Graphitic Carbon Nitride Photocatalysts: A Review

Sujana Chandrappa, Simon Joyson Galbao, Akihiro Furube, and Dharmapura H. K. Murthy*

Cite This: *ACS Appl. Nano Mater.* 2023, 6, 19551−19572

Read Online

ACCESS | Metrics & More | Article Recommendations

ABSTRACT: Due to its chemical/thermal stability, metal-free nature, abundance, low toxicity, cost-effectiveness, high surface area, tunable properties, and ease of synthesis, graphitic carbon nitride (g-C_3N_4) is a promising material for applications in catalysis, sensing, energy storage and optoelectronics. By virtue of its optical band gap, g-C_3N_4 has been extensively used to drive a range of photocatalytic reactions, such as H_2 generation, CO_2 reduction, N_2 fixation, and organic transformation, to name a few. Despite these prospects, significant improvement in extending its optical absorption is essential because g-C_3N_4 absorbs light only up to 460 nm (≈10% of the incoming sunlight). Thus, reducing its band gap to harness a wider part of the sunlight is a key approach to advancing the solar energy conversion efficiency of g-C_3N_4. In this direction, the effect of (i) improving the degree of polymerization, (ii) molecular and elemental doping, (iii) distorting planar structure, (iv) inducing nitrogen vacancies, and (v) tuning the C/N ratio of g-C_3N_4 on red-shifting the optical absorption is analyzed in detail. A comprehensive correlation between the synthesis approach/conditions−structure−optical property is established. Rational guidelines on extending the spectral response of g-C_3N_4 toward the visible/near-infrared region and using low-energy photons to drive photocatalytic reactions efficiently are detailed. The insights presented will help to utilize the full potential of g-C_3N_4 to enhance the solar fuel generation efficiency and in understanding the mechanism of light absorption.

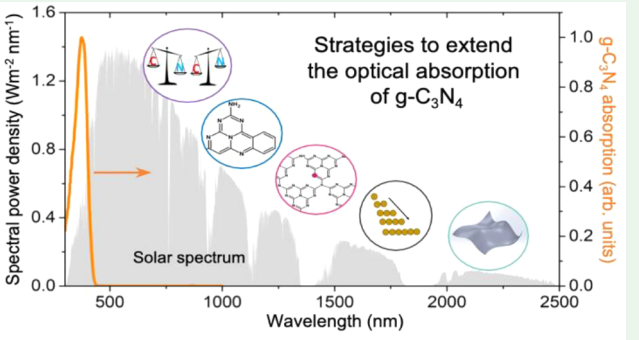

KEYWORDS: *Graphitic carbon nitride, photocatalysis, optical absorption, band gap, defects, thermal polymerization, doping, H_2 generation*

1. INTRODUCTION

Sunlight is the primary source of heat and light for life on Earth. An hour of solar irradiation on the Earth's surface will suffice for human energy consumption for over a year.[1] Driven by billions of years of evolution, nature has designed photosynthesis to efficiently harvest sunlight. It occurs commonly in green plants where CO_2 and water are converted to carbohydrates and oxygen by absorbing sunlight.[2] In efforts to mimic natural photosynthesis, a process called photocatalysis was developed at the beginning of the 20th century.[3] In photocatalysis, a semiconducting material harvests the sunlight owing to its optical band gap, essentially mimicking the role of a leaf in photosynthesis.[4] These materials generate electrons and holes upon light absorption, which can potentially be utilized for a range of reduction and/or oxidation reactions. Indeed, such reactions were possible via photocatalytic water splitting on TiO_2 surface[5] and CO_2 reduction using $BaLa_4Ti_4O_{15}$ photocatalyst.[6] There has been a significant advancement in extending the photocatalytic approach to a range of reactions like NH_3 decomposition,[7,8] biomass valorization,[9] converting waste to value-added chemicals/fuels,[10,11] and environmental remediation.[12−14]

Even after four decades of its discovery, work related to photocatalysis was limited to lab-scale research activities. The photocatalytic approach has not been transformed into a technology and its feasibility toward large-scale solar fuel production was not conceived. Domen and his group recently reported sunlight-driven H_2 generation over 100 m^2 photocatalyst modules.[15] This work demonstrated the potential and viability of the photocatalytic approach toward scalable green H_2 production for the first time. Another recent work from Mi group demonstrated solar-to-hydrogen (STH) energy conversion efficiency of 6% using seawater under direct sunlight.[16] These recent reports unambiguously demonstrate the

Received: October 5, 2023
Revised: October 12, 2023
Accepted: October 12, 2023
Published: October 31, 2023

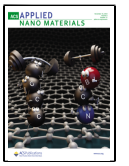

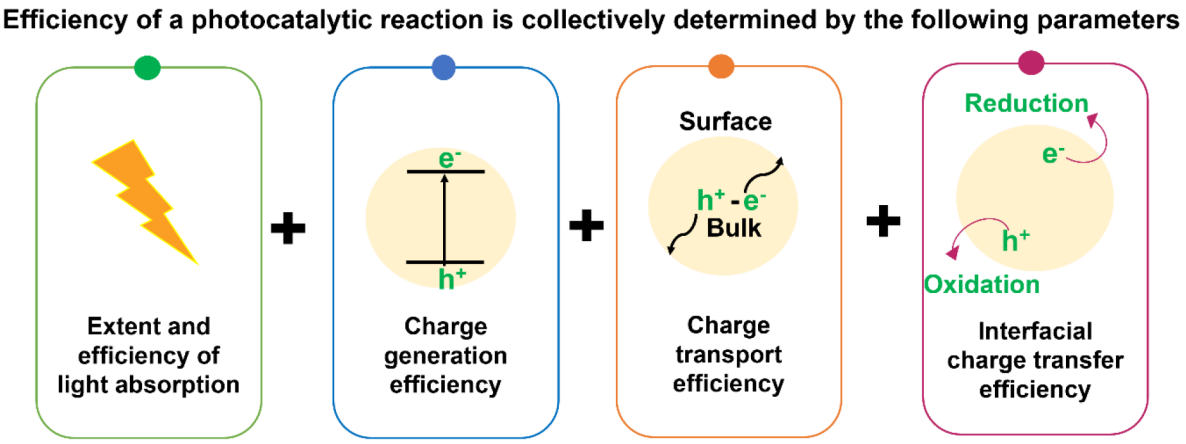

Figure 1. Factors determining the efficiency of a photocatalytic reaction.

possibility of using photocatalysis approach to generate solar fuels at scale.

The past decade has witnessed tremendous growth in photocatalytic water splitting. However, the challenge remains in designing cost-effective photocatalysts exhibiting prolonged stability under the aqueous environment. In addition, improving the ability of a photocatalyst to harness a wider part of the solar spectrum by reducing its optical band gap is critical.[17−19] Thus, there is immense scope and need to develop narrow band gap photocatalysts to enhance the STH energy conversion efficiency further.

2. FACTORS DETERMINING THE EFFICIENCY OF A PHOTOCATALYTIC REACTION

The photocatalysis process starts with the absorption of photons with energy greater than the band gap of the semiconducting photocatalyst, leading to charge carrier generation, i.e., electrons (e^-) in the conduction band and holes (h^+) in the valence band. While the photogeneration of charge carriers takes place in the bulk of the semiconductor, they must migrate to the surface of the semiconductor, which is the reaction site. Finally, interfacial electron and/or hole transfer results in reduction or oxidation reactions.[20−23] As a prerequisite, the conduction and valence bands of the photocatalyst must straddle with the reduction and oxidation potential of the target reaction.[24−26] The photocatalytic efficiency is collectively governed by the efficiency of light absorption, charge carrier generation, charge migration, and charge transfer across the semiconductor−electrolyte interface, as depicted in Figure 1.

While the efficiency of charge carrier generation, migration, and interfacial charge transfer has a definite impact on the photocatalytic performance, the initial judgment of the photocatalytic efficiency is primarily decided by the efficiency and the extent of light absorption. Metal oxides have been extensively used to drive a range of photocatalytic reactions for nearly five decades.[27−32] However, they are fundamentally limited by their light absorption capacity, exclusively in the ultraviolet (UV) region, which constitutes <5% of the solar spectrum.[33,34] The visible region (400−760 nm) constitutes ≈45% of the incoming sunlight.[35] Most photocatalysts absorbing in this range are metal-based sulfides, nitrides and oxynitrides, which suffer from poor chemical stability.[36−38] Thus, there is immense scope to develop narrow-band gap metal-free photocatalysts with extended optical absorption in the visible region and prolonged stability.

3. G-C_3N_4: A PROMISING PHOTOCATALYST WITH TUNABLE OPTOELECTRONIC PROPERTIES

Metal-free photocatalysts are semiconducting materials made up of elements such as carbon (C), nitrogen (N), oxygen (O), sulfur (S), and phosphorus (P).[39,40] Of these elements, C- and N-based polymeric semiconductors, known as graphitic carbon nitride (g-C_3N_4), is drawing immense attention due to their metal-free nature, two-dimensional (2D) polymeric structure, facile preparation method, chemical stability and optical absorption edge in the visible region. In addition, g-C_3N_4 offers a unique opportunity to tune its optoelectronic property via surface modification and doping at molecular and atomic level. Furthermore, the absorption coefficient of g-C_3N_4 thin film is ≈10^4 cm^{-1} at 430 nm,[41] which is comparable to that of conducting polymer such as poly(3-hexylthiophene).[42] Despite the absence of continuous π-conjugation in g-C_3N_4, unlike typical conducting polymers with extended conjugated networks, their optical absorption efficiency is very high. These advantages further highlight the promising prospects of g-C_3N_4 for optoelectronic applications, specifically photocatalysis.

Such prospects of g-C_3N_4 have significantly increased the number of publications, as indicated in Figure 2. Among them, more than 40% of the published reports between 2011 and 2022 are exclusively related to photocatalysis, reinforcing the immense importance of g-C_3N_4 as a photocatalyst. Photocatalytic research utilizing g-C_3N_4 was pioneered by Wang et al. in 2009 for water-splitting reaction.[43] Since then, there has been significant advancement in the design of g-C_3N_4 for various photocatalytic reduction reactions such as H_2 evolution,[44,45] CO_2 reduction,[46,47] dye degradation,[13,48] and organic transformation reactions,[49,50] depicted in Figure 3. However, limited reports on g-C_3N_4 demonstrate oxidation reactions promoted by direct hole oxidation.[51] This is because g-C_3N_4 does not have the required thermodynamic driving energy to form hydroxyl free radicals (oxidants).[52,53] Besides its utilization in photocatalysis, g-C_3N_4 is explored for sensing, light-emitting diodes and imaging that harnesses its photoluminescent (PL) property.[54−57]

The feasibility of photocatalytic reaction at scale (≈1 m^2) using g-C_3N_4 photocatalyst has already been demonstrated by Schröder et al.[58] Figure 4 depicts a panel-type reactor consisting of Pt-loaded mesoporous g-C_3N_4 drop-casted onto

https://doi.org/10.1021/acsanm.3c04740
ACS Appl. Nano Mater. 2023, 6, 19551−19572

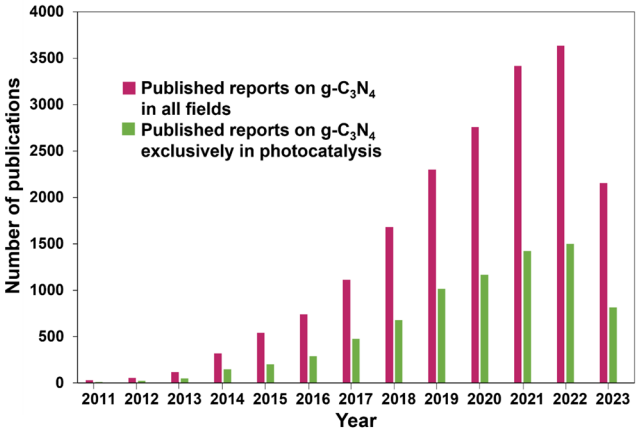

Figure 2. Statistics derived from the Web of Science database on the number of publications on g-C_3N_4 from 2011 to 2023. The keywords used were "g-C_3N_4" and "g-C_3N_4 + photocatalyst". The date of search is 10th September 2023.

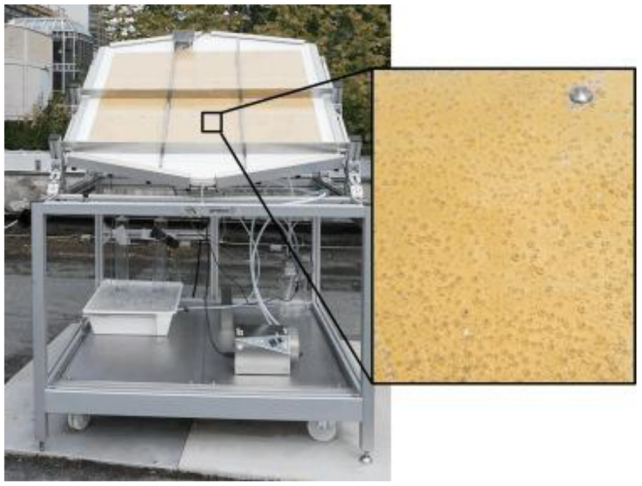

Figure 4. Large-scale solar H_2 evolution reaction demonstrated using a panel-type reactor containing immobilized Pt-loaded mesoporous carbon nitride photocatalyst. H_2 evolution (bubbling) on the surface of photocatalysts is shown in the magnified image. Reproduced with permission from ref 58. Copyright 2015 John Wiley and Sons.

stainless steel. In 30 days, 18.2 L of H_2 was generated from 0.756 m^2 photocatalyst panel. However, the STH energy conversion efficiency achieved was 0.12%, which is still very low compared to the theoretical maximum efficiency of ≈5%.[59] Thus, there is immense scope to understand the optoelectronic property further to enhance the STH energy conversion efficiency of g-C_3N_4.

Despite such extensive investigations, the main challenge is to improve the light absorption efficiency of g-C_3N_4. In addition, due to inadequate correlation between the synthesis−structure−property of g-C_3N_4, our understating of the mechanism of light absorption is limited. The absorption onset of g-C_3N_4 is around 460 nm, narrowly qualifies as a visible-light absorbing photocatalyst. Figure 5 compares the solar and the optical absorption spectrum of strontium titanate ($SrTiO_3$), g-C_3N_4 and tantalum nitride (Ta_3N_5). The light-harvesting capacity of g-C_3N_4 exceeds that of wide band gap $SrTiO_3$, which absorbs only in the UV region.[60] However, g-C_3N_4 can absorb up to 460 nm, which only accounts for ≈10% of the incoming sunlight. On the other hand, Ta_3N_5 absorbs up to ≈620 nm, thus harvesting an additional ≈25% of the solar spectrum relative to g-C_3N_4. The theoretical maximum STH energy conversion efficiencies[59] of these photocatalysts are also compared in Figure 5. A further red-shift of the absorption of g-C_3N_4 is key to achieving higher STH energy conversion efficiency and will help utilize its promising prospects. In this direction, this Review offers an overall perspective of the existing routes/methods to intrinsically reduce the optical band gap of g-C_3N_4 that allows the harvesting of low-energy photons of sunlight.

3.1. Chemical Structure and Synthesis of g-C_3N_4. According to the first-principles density functional theory

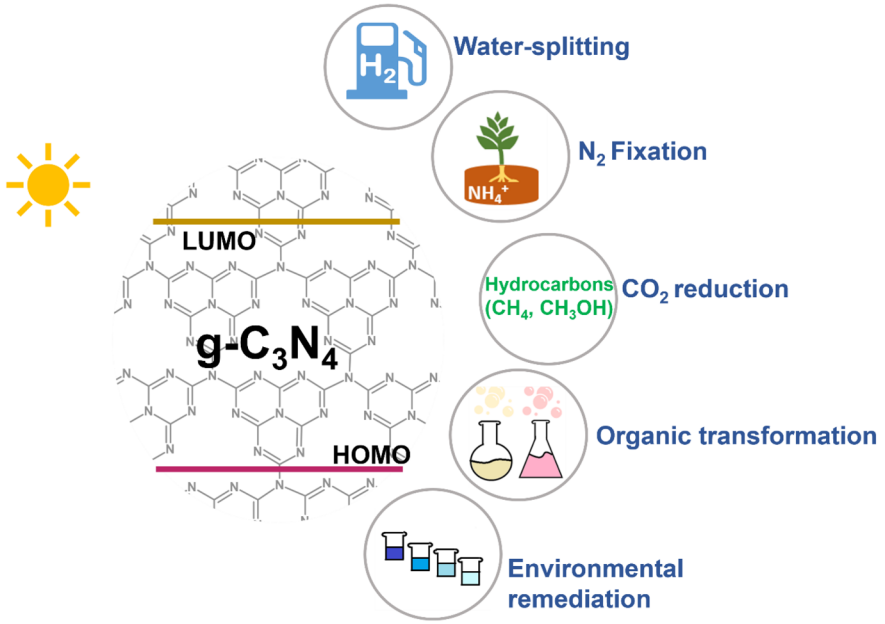

Figure 3. Applications of g-C_3N_4 in various reduction and/or oxidation reactions via the photocatalytic approach.

https://doi.org/10.1021/acsanm.3c04740
ACS Appl. Nano Mater. 2023, 6, 19551−19572

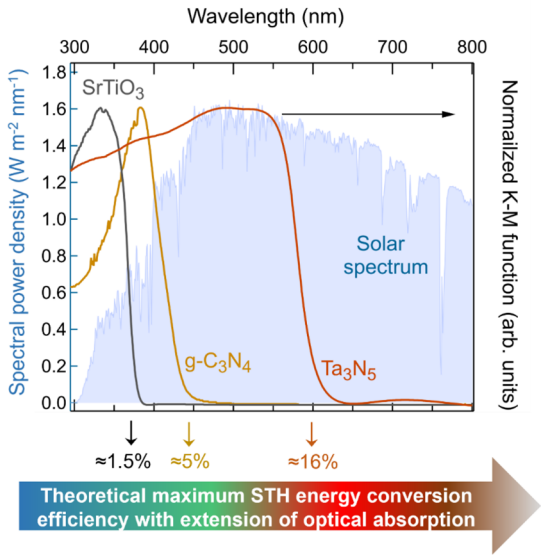

Figure 5. Comparing the solar spectrum and the optical absorption spectra (right axis) of $SrTiO_3$, g-C_3N_4, and Ta_3N_5 powdered photocatalysts measured in diffuse reflection mode. Theoretical maximum STH energy conversion efficiency of the photocatalysts is mentioned below the spectral overlay. Note that the solar spectrum is shown only to 800 nm to allow better comparison.

(DFT) studies, C_3N_4 has seven phases, namely, α-C_3N_4, β-C_3N_4, cubic C_3N_4, pseudocubic, and graphitic phases (g-h-triazine, g-h-heptazine, and g-o-triazine).[61] Either triazine or tri-s-triazine-based rings with interconnected planar amino groups form the tectonic units of the allotropes of g-C_3N_4, as depicted in Figure 6a and 6b.[62] g-C_3N_4 has a layered structure similar to graphite where the stacking layers are held together by weak van der Waals forces. Each layer of g-C_3N_4 contains carbon and nitrogen atoms arranged in an alternate fashion connected by alternating double bonds within the triazine and/or tri-s-triazine unit (also known as heptazine). In addition, Figure 6c and 6d demonstrates another class of carbon nitrides-poly(heptazine imide) (PHI) and poly(triazine imide) (PTI), respectively. In PHI, heptazine units are connected by imide groups, bonded to three neighboring heptazine units. Such an arrangement of heptazine units creates a triangular void that is stabilized by a melamine molecule through hydrogen bonding (H-bonding).[63] The unique structure of PHI is achieved through a synthesis process that involves further polymerization of partially condensed melon using salt melts.[64] On the other hand, PTI features a completely delocalized π-electron system with triazine units linked by imide groups, as depicted in Figure 6d. It is synthesized using eutectic LiCl and KX (X: Cl or Br) salt melts with C- and N-

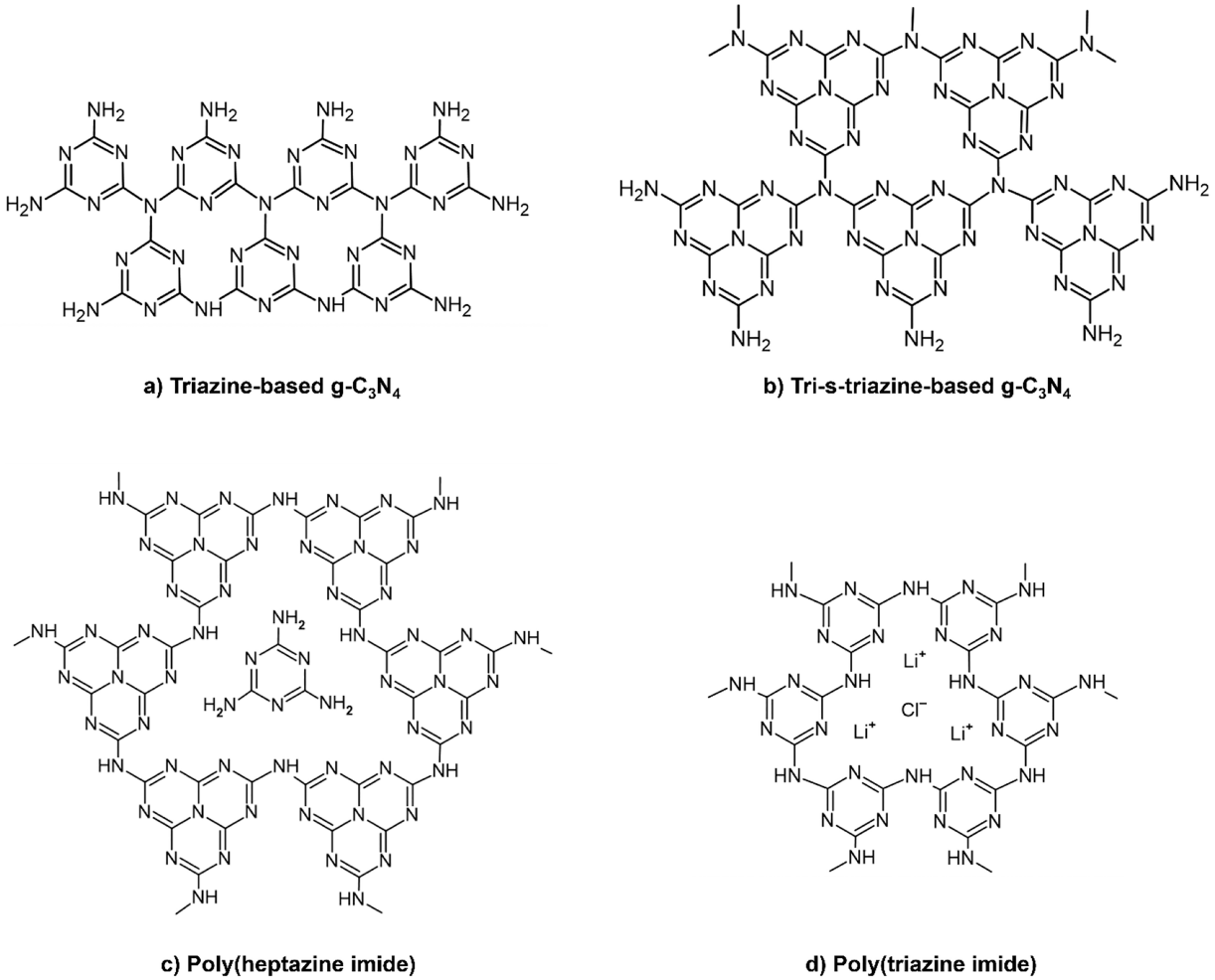

Figure 6. g-C_3N_4 comprised of (a) triazine units, (b) tri-s-triazine units, (c) poly(heptazine imide) units, and (d) poly(triazine imide) units.

https://doi.org/10.1021/acsanm.3c04740
ACS Appl. Nano Mater. 2023, 6, 19551−19572

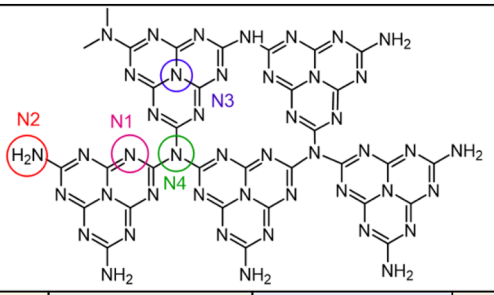

FTIR		^{15}N solid-state NMR		N 1s XPS		Raman spectroscopy	
≈800 cm^{-1}	Breathing mode of tri-s-triazine units	≈200 ppm	N1	≈398.6 eV	N1	≈1200-1700 cm^{-1}	Stretching mode of tri-s-triazine ring
≈1200-1400 cm^{-1}	Stretching vibration mode of C-N	≈137-110 ppm	N2	≈399.8 eV	N2		
≈1550-1640 cm^{-1}	Stretching vibration mode of C=N	≈157 ppm	N3	≈401.0 eV	N3/N4	≈810 cm^{-1}	Breathing mode of tri-s-triazine units
≈3000-3500 cm^{-1}	Stretching modes of –NH/NH$_2$ groups						

Figure 7. Tri-s-triazine-based g-C_3N_4 indicating the types of N atoms involved in bonding, indicated as N1, N2, N3, and N4. Experimental evidence confirming the chemical structure of tri-s-triazine-based units of the g-C_3N_4 obtained from FTIR, ^{15}N solid-state NMR, XPS, and Raman spectroscopy analysis are mentioned.[75−80]

rich precursors, where Li^+ and Cl^- are intercalated into the triazine-based structure.[65]

Among all phases, tri-s-triazine-based g-C_3N_4 is the most stable one reported for carbon nitride. Figure 7 shows four nonequivalent N atoms in the tri-s-triazine unit are present—one (N1) is two-coordinated, while three N atoms (N2, N3, N4) are three-coordinated. The chemical and electronic nature of tri-s-triazine units of g-C_3N_4 can be characterized by Fourier transform infrared (FTIR), Raman spectroscopy, ^{15}N solid state-nuclear magnetic resonance (NMR) and X-ray photoelectron spectroscopy (XPS),[75−80] as detailed in Figure 7. A strong covalent interaction between C and N atoms in the heterocyclic tri-s-triazine units renders thermal (up to 600 °C) and chemical stability. In addition, due to the conjugated electronic structure of sp^2 hybridized C and N within the tri-s-triazine units, it has the lowest band gap (≈2.75 eV) among all the phases of carbon nitride, thus capable of harvesting visible light.[43,81−83]

g-C_3N_4 was first synthesized via the thermal polymerization of cyanamide between 400 to 600 °C and employed as a photocatalyst for the H_2 evolution reaction.[43] Typically, the polymerization of cyanamide to dicyanamide and melamine occurs between 200 to 240 °C. A further rise in temperature to 390 °C led to the rearrangement of melamine units to form tri-s-triazine-based units, which subsequently polymerized to form g-C_3N_4 around 520 °C. However, prolonged heating of g-C_3N_4 beyond 600 °C led to the disintegration of the g-C_3N_4 structure. Table 1 lists various precursors and methods employed in the synthesis of g-C_3N_4 along with the resulting band gap. It clearly shows the effect of temperature and precursor on the optical property of g-C_3N_4, which can be utilized to tune its optoelectronic properties. Depending on the precursor, the intermediates formed in the initial stage and the pathway of the g-C_3N_4 formation differ.[43,84,85] Figure 8 depicts various reaction intermediates formed during the synthesis of g-C_3N_4.[86] However, most reports indicate that polymerization proceeds via the formation of melon units, indicating that tri-s-triazine is the building block of polymeric g-C_3N_4.[84,87−90]

Table 1. Different Preparation Methods, Precursors Employed, Temperature Range Utilized in the Synthesis of g-C_3N_4, and the Resulting Band Gap

Synthesis method	Precursor(s)	Temperature (°C)	Band gap (eV)	Ref.
Thermal polymerization	Melamine	580	2.75	66
	Urea	520−550	2.73	67
	Dicyandiamide	550	2.66	67
	Thiourea	550	2.60	67
	Cyanamide	500	2.62	68
Chemical vapor deposition	Melamine	600	2.87	69
	Melamine	550	2.88	70
	Melamine	550	NA	71
Solvothermal synthesis	Cyanuric acid, sodium azide, acetonitrile	220	1.85	72
	Cyanuric acid, sodium azide, acetonitrile	180	2.51	73
Physical vapor deposition	Graphite and N_2/Ar discharge	NA	NA	74

3.2. Electronic Structure and Optical Absorption. The ability of the conjugated polymers to absorb UV−visible light is attributed to the sp^2-hybridization of the elements in the conjugated system.[91] The N and C atoms in the tri-s-triazine unit of g-C_3N_4 are sp^2-hybridized. Hence, initially, single electron-filled p_z orbitals of C and N atoms split into two energy bands, corresponding to π and π^* of bonding and antibonding nature, respectively. The first-principles study indicated that the highest occupied molecular orbital (HOMO) mainly comprises N 2p and N 2s orbitals with a minor contribution from C 2p and C 2s orbitals. On the other hand, the lowest unoccupied molecular orbital (LUMO) primarily consists of C 2p and N 2p orbitals.[92]

https://doi.org/10.1021/acsanm.3c04740
ACS Appl. Nano Mater. 2023, 6, 19551−19572

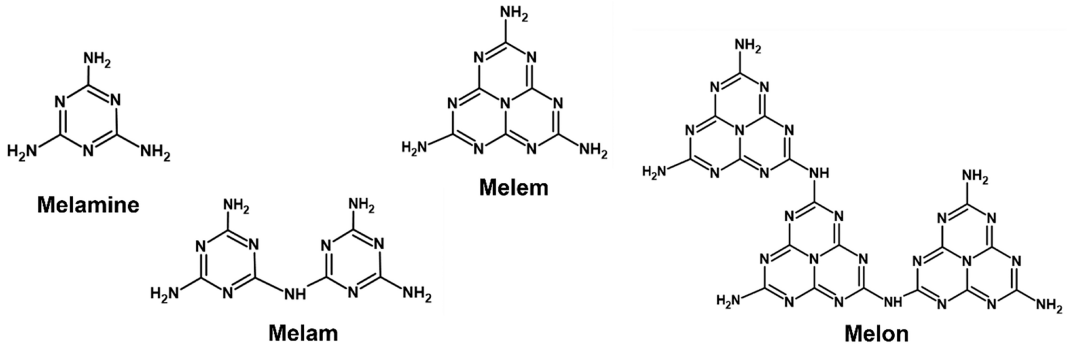

Figure 8. Various intermediates formed during the thermal polymerization of C- and N-rich precursors.[86]

Theoretically, two types of electron transitions are possible in g-C_3N_4, (i) $\pi \rightarrow \pi^*$ and (ii) $n \rightarrow \pi^*$. Upon light absorption, electrons are excited from π orbitals (HOMO) to π^* (LUMO), constituting the fundamental transition, depicted as T_1 in Figure 9. The energy requirement for T_1 gives rise to an absorption onset of ≈460 nm, as shown in Figure 5.[91] The transitions from lone pair of electrons on the edge N atoms (N1 in Figure 7) to π^* orbitals are theoretically predicted to yield an absorption shoulder at $\lambda \geq 490$ nm.[92] This transition is denoted as T_2 in Figure 9. However, $n \rightarrow \pi^*$ electron transitions are rarely reported in a perfectly symmetric, planar g-C_3N_4, likely because a lone pair of electrons on N atoms lie orthogonal to the π-conjugation plane and cannot be photoexcited. Therefore, $\pi \rightarrow \pi^*$ is the transition responsible for visible-light absorption, resulting in a band gap of ≈2.75 eV. In the subsequent sections, various approaches to red-shift ($\lambda \geq 460$ nm) the optical absorption of g-C_3N_4 will be discussed.

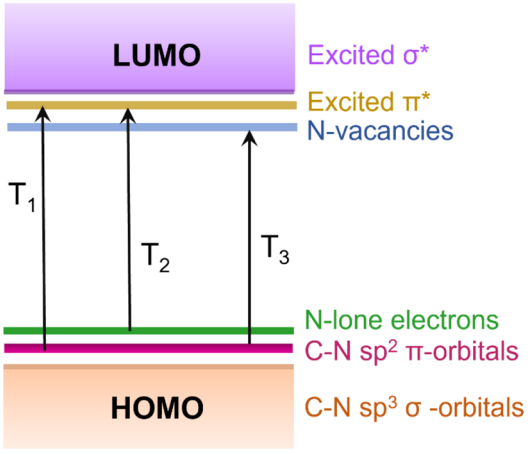

Figure 9. Proposed energy band diagram of g-C_3N_4 indicating fundamental transition (T_1) and possible transitions (T_2 and T_3) at a lower energy than T_1.

4. OPPORTUNITIES TO RED-SHIFT THE OPTICAL ABSORPTION OF G-C_3N_4 BEYOND 460 NM FOR EFFICIENT UTILIZATION OF THE SOLAR SPECTRUM

There have been attempts to extend the optical absorption of g-C_3N_4 by making its composite (or heterostructure) with another near-infrared (NIR) absorbing material. This approach has been used in *z*-scheme photocatalysis reactions.[93−97] However, despite significant research progress, a mechanistic insight into intrinsically red-shifting the optical absorption of g-C_3N_4 is limited. In addition, understanding of how the

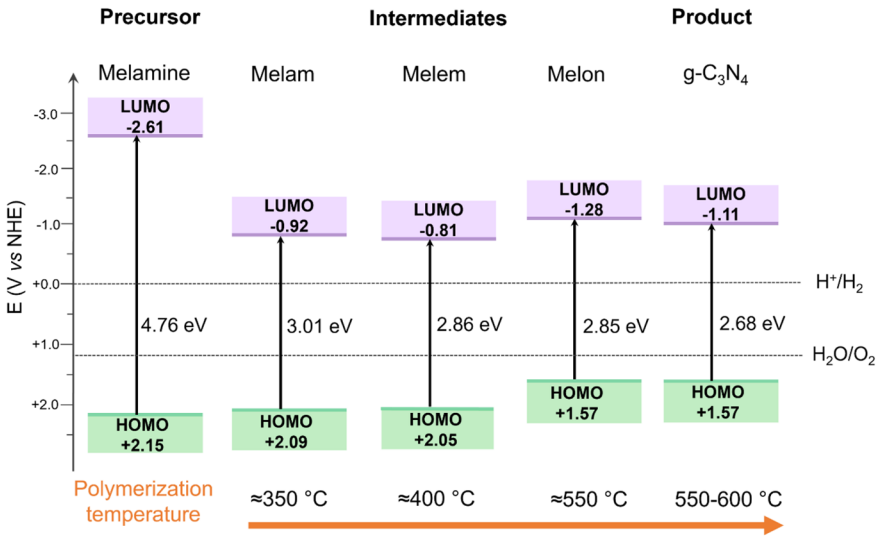

Figure 10. Band gap, HOMO−LUMO positions of precursor, intermediates, and the product (g-C_3N_4) formed during the polymerization of C- and N- rich precursor (melamine). Adopted from multiple references.[98−100]

https://doi.org/10.1021/acsanm.3c04740
ACS Appl. Nano Mater. 2023, 6, 19551−19572

Table 2. Copolymerization of C- and N-Precursors with Different Types of Comonomers and the Resulting Changes in Optoelectronic Properties[a]

Comonomer	Proposed product from copolymerization	Effect on the electronic structure that red-shifted optical absorption
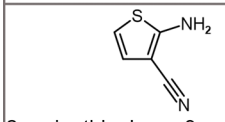 2-aminothiophene-3-carbonitrile (ATCN)	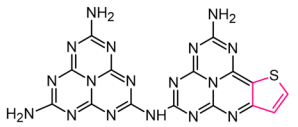	Electron donation and extended conjugation
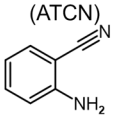 2-aminobenzonitrile (ABN)	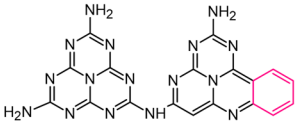	Extended aromatic conjugation
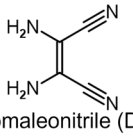 Diaminomaleonitrile (DAMN)	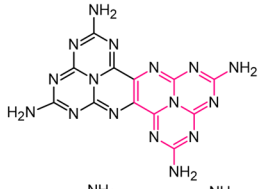	Promotes extended conjugation in -C=N-
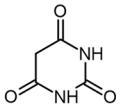 Barbituric acid (BA)	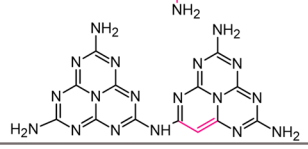	Improved -C=C- conjugation compared to -C=N-

[a]Structural changes induced in the tri-s-triazine unit due to copolymerization are highlighted in pink.

synthesis approach determines the optical properties is limited. In this direction, this Review aims to establish a correlation between various synthesis parameters/conditions with the resulting chemical structure and its optoelectronic properties. A critical outlook and approaches on band gap engineering to intrinsically extend its spectral response toward visible/NIR region is offered. Considering the scope of this Review, reports on red-shifting the optical response by forming composites or heterojunctions with other materials are not discussed.

From the preliminary understanding of the energy band structure of g-C_3N_4, three routes to red-shifting the optical absorption are recognized. The $\pi \rightarrow \pi^*$ is an allowed transition making g-C_3N_4 visible-light ($\lambda \leq 460$ nm) active. Therefore, the primary strategy to extend the optical absorption is (i) to increase the density of states (DOS) in π and π^* orbitals (T_1 in Figure 9). The energetic position of the lone pair of electrons on the edge N atoms within the tri-s-triazine rings is above the π orbitals constituting the HOMO. Therefore, (ii) enabling n $\rightarrow \pi^*$ transition at lower energy ($\lambda > 460$ nm) absorption, as indicated by T_2 in Figure 9, can significantly red-shift the optical absorption. Besides this, (iii) eliciting electron transition from HOMO to the unoccupied vacancies below the LUMO can yield red-shifted absorption ($\lambda > 460$ nm), illustrated as T_3 in Figure 9. The propositions mentioned above are realized by employing an appropriate synthesis procedure to promote a specific electron transition. In this regard, six approaches to red-shift optical absorption are identified and comprehensively analyzed. Relevant reports for each method are detailed with examples in the following subsections.

4.1. Increasing the Degree of Polymerization in Pristine g-C_3N_4. Figure 10 depicts band gap variation of the intermediates formed during the polymerization of C- and N-precursor (melamine), arranged in the increasing order of degree of polymerization (left to right). As the melamine is heated, various intermediates (refer to Figure 8) are formed, finally forming g-C_3N_4. The temperature requirement (350−600 °C) and thermal treatment duration differ from one intermediate to another and also on the precursor. While melam and melem formation from melamine required 350 and 400 °C, respectively,[98] melon was formed when melamine was heated at 550 °C for 2 h.[99] Another work revealed that a longer duration of thermal treatment of melamine at 550 °C further promoted the degree of polymerization, resulting in the formation of g-C_3N_4.[100] The band energy diagram of the g-C_3N_4 illustrated in Figure 10 evidence that the degree of polymerization in g-C_3N_4 is enhanced upon increasing the temperature up to 600 °C.

g-C_3N_4 synthesis from the thermal polymerization of urea proceeds via the formation of melamine in 250−350 °C range.[86] Further, the polymerization of melam units to tri-s-triazine-based g-C_3N_4 occurred at around 500−550 °C. The X-ray diffraction (XRD) analysis demonstrated pronounced crystallinity on increasing synthesis temperature, attributed to improved periodicity of tri-s-triazine units in melon-based g-C_3N_4. Therefore, synthesis temperature promotes the degree of polymerization, consequently increasing the DOS in HOMO and LUMO. As a result, a red-shift in the optical absorption is expected, leading to a reduced band gap.[101] Therefore, notable efforts are invested in increasing the degree of polymerization in g-C_3N_4 to reduce the band gap.

Temperature-dependent polymerization of g-C_3N_4 films was recently evidenced by Chubenko et al. using the chemical vapor deposition (CVD) technique.[69] g-C_3N_4 films on glass substrates were synthesized at 550, 600, and 625 °C. An evident improvement in the crystallinity of the samples was observed when the temperature was increased from 550 to 600 °C owing to the increased degree of polymerization. Polymerized tri-s-triazine units were found in maximum concentration when synthesized at 600 °C. With a further increase in temperature (>650 °C), these units disintegrated before reaching the substrates, while below 600 °C, there was

https://doi.org/10.1021/acsanm.3c04740
ACS Appl. Nano Mater. 2023, 6, 19551−19572

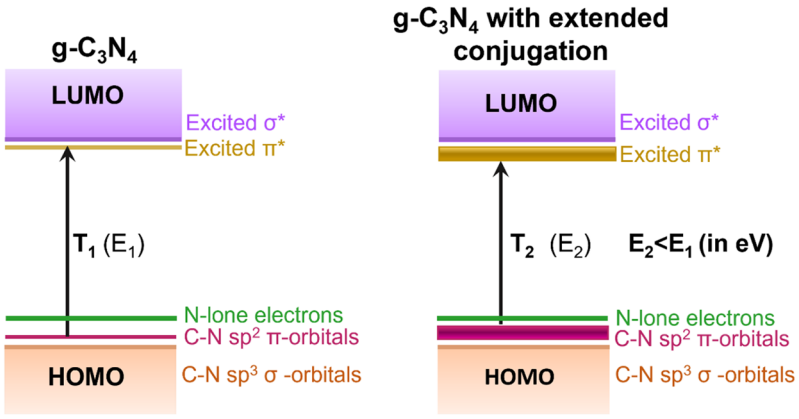

Figure 11. Proposed change in the energy band diagram of g-C_3N_4 due to copolymerization depicting the fundamental transition and energy requirement for the same in two cases.

incomplete polymerization. Therefore, synthesis temperature significantly affects the polymerization process. A transformation of the electronic band structure from the σ- to π-conjugated system was observed when the synthesis temperature was increased up to 600 °C. Therefore, the optical band gap decreased from 3.03 to 2.83 eV with the rise in temperature from 550 to 625 °C, which can be attributed to the pronounced $\pi \rightarrow \pi^*$ transition, illustrated as T_1 in Figure 9.

The effect of temperature on the polymerization of C- and N- rich precursors into g-C_3N_4 was also evidenced in powder samples. g-C_3N_4 synthesized from precursors such as melamine at different temperatures exhibited improved crystallinity with increasing temperature to 550 °C. This observation was consistent with a noticeable red-shift in optical absorption and a visible change in the color of the g-C_3N_4.[66,102] While increasing the synthesis temperature resulted in the polymer growth in several reports, increasing temperature beyond 550 °C blue-shifted the optical absorption of g-C_3N_4, synthesized from thiourea.[85] This was attributed to the decomposition of the g-C_3N_4 into smaller particles, which may have induced a quantum confinement effect, supported by surface area analysis. To this end, it can be inferred that the polymerization temperature (350−600 °C) plays a significant role in promoting the condensation of C- and N-rich precursors, forming various intermediates, eventually forming polymeric g-C_3N_4. Therefore, with the polymerization of more tri-s-triazine units, a pronounced $\pi \rightarrow \pi^*$ transition is observed, resulting in a red-shifted optical absorption, as discussed in this section. On the other hand, heating beyond 650 °C reduced the band gap due to the disintegration of g-C_3N_4, resulting in the quantum confinement effect. Thus, polymerization temperature plays a crucial role in controlling the optical properties of g-C_3N_4.

4.2. Extending the Degree of Conjugation by Copolymerization/Molecular Doping. Section 4.1 illustrated the effect of temperature on the polymerization of g-C_3N_4, which influences the extent of optical absorption. Another route to extending the optical absorption is via copolymerization, known as molecular doping of precursors with another organic molecule (comonomer). The desired change in electronic properties can be incorporated into the tri-s-triazine units by rationally selecting the appropriate comonomer. By increasing the extent of conjugation, a reduction in the g-C_3N_4 band gap is expected.

Incorporating comonomers into the tri-s-triazine units of the g-C_3N_4 influenced the electronic properties and consequently the energy band structure, as depicted in Table 2. The copolymerized g-C_3N_4 showed extended conjugation leading to improved light absorption efficiency compared to the pristine g-C_3N_4.[103] Figure 11 depicts the proposed change in the energy band diagram of g-C_3N_4 upon copolymerization with organic molecules. The effect of four comonomer molecules, namely, barbituric acid (BA), 2-aminobenzonitrile (ABN), 2-aminothiophene-3-carbonitrile (ATCN), diaminomaleonitrile (DAMN), on the optical absorption of g-C_3N_4 synthesized from dicyanamide were studied.[103] Interestingly, incorporating organic structures did not destroy the structural integrity of g-C_3N_4. A red-shift of optical absorption for all four copolymerized samples was observed, with an additional pronounced absorption shoulder in 450−600 nm range for g-C_3N_4 copolymerized with ABN, ATCN and DAMN.

Copolymerization of urea with BA resulted in a substitution of an N atom by a C atom in the form of −C═C− in the tri-s-triazine unit, as depicted in Table 2.[103] This resulted in a marginal red-shift of optical absorption, which may be attributed to the lower amounts of BA incorporation. Nonetheless, it still indicates that substituting of N by C alters the electronic structure of g-C_3N_4. Similarly, BA copolymerized g-C_3N_4 introduced −C═C−H functionality, extending absorption toward 530 nm.[104] The improved photocatalytic efficiencies can be attributed to the extended light absorption of the photocatalyst. Furthermore, when dicyanamide was copolymerized with BA, similar results were obtained by another group.[105] An evident red shift in optical absorption up to 650 nm was observed with an increase in the amount of BA, indicating the improvement in electron delocalization upon copolymerization with BA.

Copolymerization of urea with ABN inserted benzene in the tri-s-triazine unit and red-shifted the optical absorption up to 600 nm.[103] Similar red-shift in the optical absorption up to ≈700 nm were realized by several other groups as well.[106,107] In another work, benzene was incorporated in g-C_3N_4 by polymerization of urea with *N*-phenylthiourea.[108] Benzene is proposed to substitute for the triazine unit in the tri-s-triazine structure, which resulted in a red shift of absorption to 482 nm with an absorption shoulder appearing in the range 450 to 700 nm. Such extended absorption can be attributed to the improved −C═C− conjugation in than −C═N−, which also enhanced charge transfer efficiency. Benzene incorporation in the g-C_3N_4 structure enhanced the photocatalytic H_2 evolution rate by ≈8 times compared to pristine g-C_3N_4. On the other

https://doi.org/10.1021/acsanm.3c04740
ACS Appl. Nano Mater. 2023, 6, 19551−19572

Table 3. Effect of Copolymerization on the Optical Absorption and Photocatalytic H_2 Evolution Efficiency of g-C_3N_4

Precursor	Comonomer	Bandgap (eV)		H_2 evolution rate		Ref.
		Before	After	Before	After	
Urea	Benzenesulfonic acid	2.59	2.32	≈2.68 mmol g^{-1} h^{-1}	7.25 mmol g^{-1} h^{-1}	117
	2-Aminobenzimidazole	2.68	2.46	951 μmol g^{-1} h^{-1}	2566 μmol g^{-1} h^{-1}	118
Melamine + cyanuric chloride	Triaminotriphenylamine	2.37	2.32	9158.5 μmol g^{-1} h^{-1}	16897.3 μmol g^{-1} h^{-1}	119
Urea	*N*-Phenylthiourea	2.73	2.57	339.16 μmol g^{-1} h^{-1}	2791.4 μmol g^{-1} h^{-1}	108
	2,5-Dibromopyrimidine	2.73	2.70	213.9 μmol g^{-1} h^{-1}	3279.7 μmol g^{-1} h^{-1}	120
Melamine	Glucose	2.63	2.52	160 μmol g^{-1} h^{-1}	7581 μmol g^{-1} h^{-1}	121
Urea	2-aminoterephthalic acid	2.94	2.86	3323 μmol $g^{-1}h^{-1}$	10600 μmol $g^{-1}h^{-1}$	122
Dicyandiamide	Barbituric acid	2.67	2.57	6.5 μmol h^{-1}	29.4 μmol h^{-1}	105
	3-Aminothiophene-2-carbonitrile	2.72	2.66	13.4 μmol h^{-1}	131 μmol h^{-1}	110
Urea	1,3,5-Tris(4-aminophenyl)benzene	2.85	2.82	42 μmol h^{-1}	211 μmol h^{-1}	111
	Benzamide	2.63	2.51	0.75 mmol g^{-1}	2.38 mmol g^{-1}	112
	3-Aminobenzoic acid	2.84	2.78	26.1 μmol h^{-1}	104.0 μmol h^{-1}	113
	6-Aminopyridine-2-carboxylic acid		2.80		133.2 μmol h^{-1}	

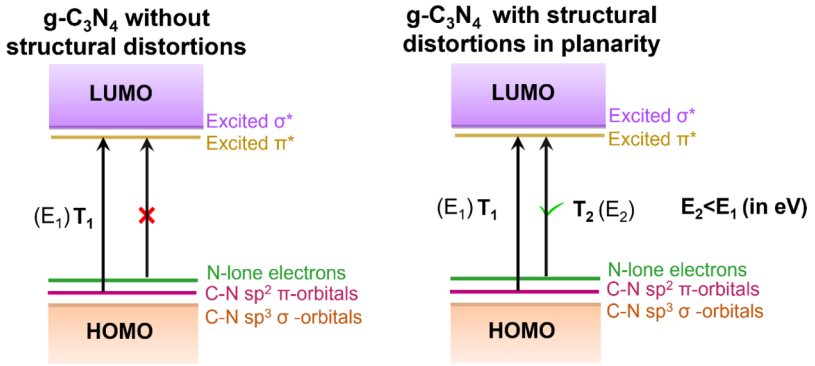

Figure 12. Proposed energy band diagram of planar g-C_3N_4 and g-C_3N_4 with structural distortions in planarity, indicating that the n → π^* transitions are enabled in the latter.

hand, copolymerizing urea with another comonomer, DAMN resulted in an extended conjugation via promoting covalent bonding between two tri-s-triazine units, as shown in Table 2. Copolymerization of urea with ATCN resulted in the insertion of the thiophene unit in the tri-s-triazine unit.[103] The marginal red shift in the intrinsic $\pi \rightarrow \pi^*$ transition may be attributed to the extended conjugation owing to the thiophene unit. In addition, an absorption around 450−550 nm may be ascertained to the electron transition from the lone pair of electrons on sulfur (present in the thiophene unit) to the π^* orbitals. Similar observations were made by several other groups as well.[109,110] Wavelength-dependent H_2 evolution data confirms that lower energy photons (λ > 460 nm) are effectively utilized to realize H_2 generation due to pronounced $\pi \rightarrow \pi^*$ transition.[110] Similarly, 1,3,5-tris(4-aminophenyl)-benzene,[111] benzamide,[112] 6-aminopyridine-2-carboxylic acid, and 2-aminobenzoic acid[113] are copolymerized with C- and N-rich precursors which resulted in a marginal extension of the optical absorption ($\lambda \leq$ 500 nm).

Furthermore, polycyclic aromatic hydrocarbons (PAHs) such as naphthalene, anthracene, and pyrene were used as comonomers to increase the degree of conjugation in g-C_3N_4. Introducing such PAHs red-shifted the optical absorption and enhanced the charge photogeneration yield.[114,115] For example, naphthalene-incorporated g-C_3N_4 enhanced the photocatalytic H_2 evolution rate by a factor of 2 compared to pristine g-C_3N_4. However, introducing bulkier anthracene and pyrene units distorted the g-C_3N_4 structure and consequently decreasing the photocatalytic performance. Hence, careful control over the size and location of PAHs incorporation to g-C_3N_4 is critical.

Recently, the incorporation of the C-ring (C_r) network into the g-C_3N_4 was found to improve the extent of conjugation. Wu et al. reported porous g-C_3N_4 with a honeycombed structure synthesized via the CVD process with copyrolysis of glucose and melamine using SiO_2 nanospheres as a template.[116] At a CVD temperature ≥320 °C, glucose molecules pyrolyzed into C_r and melamine polymerized into triazine units on SiO_2 nanospheres. With the further increase in temperature to 400 °C, the C-rings and triazine units began to polymerize, forming triazine@C_r heterostructure. Finally, further polymerization of triazine@C_r units took place at 550 °C, leading to the seamless splicing of the C-ring in the carbon nitride network obtained by dissolving the template. With the in-plane splicing of C-ring in g-C_3N_4, the extent of conjugation was improved, which manifested as a red-shift in optical absorption (λ > 460 nm). These low-energy photons were also capable of H_2 evolution.[116] Therefore, strategic splicing of C_r into the g-C_3N_4 plane extended the conjugation length of g-C_3N_4, leading to a pronounced $\pi \rightarrow \pi^*$ transition, thus red-shifting the absorption (as T_2 in Figure 11).

This section highlights copolymerization as a promising approach to extending the optical absorption in g-C_3N_4 beyond 460 nm by extending the degree of conjugation, which may increase the DOS in the HOMO and LUMO edges leading to the pronounced $\pi \rightarrow \pi^*$ transition, as depicted by T_2 in Figure 11. Furthermore, several reports discussed demonstrate that the low energy (λ > 460 nm) photons

https://doi.org/10.1021/acsanm.3c04740
ACS Appl. Nano Mater. 2023, 6, 19551−19572

Table 4. Structural Distortion Induced n → π* Transitions in g-C_3N_4, Its Effect on the Band Gap, and Photocatalytic H_2 Evolution Efficiency

		Bandgap (eV)		H_2 evolution rate		
Precursor	Approaches to induce structural distortion	Before	After	Before	After	Ref.
Melamine	Post-calcination thermal treatment under N_2 atmosphere	2.66	2.47	≈25 μmol g^{-1} h^{-1}	≈90 μmol g^{-1} h^{-1}	127
Urea	Thermal exfoliation and polymerization with 2,5-dibromopyrazine	2.64	2.53	9 μmol h^{-1}	63 μmol h^{-1}	128
	Post-calcination thermal treatment under N_2 atmosphere	2.75	2.45	≈1280 μmol g^{-1} h^{-1}	9230 μmol g^{-1} h^{-1}	129
	Thermal polymerization under Ar atmosphere	2.86	2.80	224.09 μmol g^{-1} h^{-1}	454.94 μmol g^{-1} h^{-1}	130

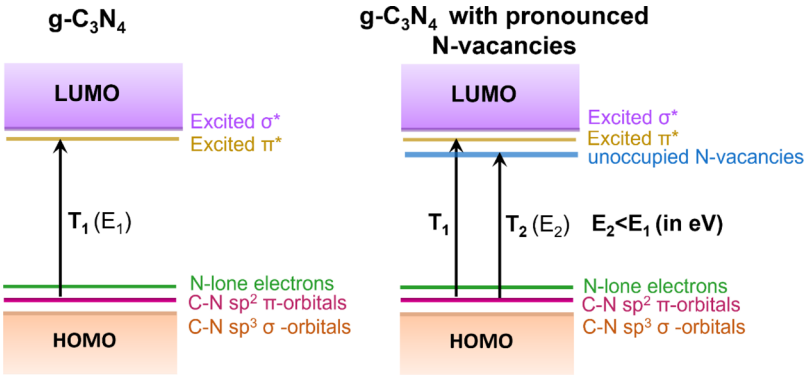

Figure 13. Proposed energy band diagram of g-C_3N_4 without and with N-vacancies indicating additional electron transitions, T_2 from π → N-vacancies at a lower energy than T_1.

harvested could populate the LUMO with free electrons, which were subsequently utilized for H_2 evolution. Table 3 lists selected comonomers used for copolymerization with precursors and their effect on the optical band gap and photocatalytic H_2 generation efficiency.

4.3. Enabling n → π* Transitions by Introducing Structural Distortions. g-C_3N_4 is a 2D layered semiconductor where each layer consists of alternating C and N atoms connected to form a tri-s-triazine unit. As mentioned in section 3.2, the electron transitions from the lone pair of electrons belonging to the sp^2-hybridized two-coordinated N atoms (N1 in Figure 7) of the tri-s-triazine units cannot be photoexcited to the π* orbitals. These electron transitions are forbidden for a perfectly symmetric planar system.[123,124] Nonetheless, significant efforts dedicated to promote n → π* transitions by inducing structural distortions in g-C_3N_4. As a result, the lone pair of electrons are now in a plane from which electron transitions to π* orbitals are possible. Figure 12 shows the expected change in the energy band structure of g-C_3N_4 due to structural distortions.

The approaches to induce structural distortions involve post-synthesis thermal treatment or exfoliation of the g-C_3N_4. Post-calcination thermal treatment of g-C_3N_4 in the H_2 atmosphere induced structural distortion in g-C_3N_4.[125] Introduction of amino groups in the tri-s-triazine structures because of H_2 reduction promoted H-bonding between the g-C_3N_4 layers. As a result, a marginal distortion of the planar structure was proposed to increase the electron density of g-C_3N_4 by enabling electron transitions from n to π* orbitals. These structural changes collectively resulted in an absorption shoulder around 460−700 nm. Similar observations are reported by other groups as well.[126,127] The effect of temperature during the postcalcination thermal treatment on promoting electron transition from n to π* orbitals was investigated by Chen et al.[92] Increasing the temperature from 550 to 625 °C did not promote n → π* transitions but improved the degree of polymerization. On the other hand, an absorption shoulder ≈500 nm appeared when the synthesis temperature was 650 °C, which was assigned to the possibility of n → π* transitions because of the buckled configuration of the g-C_3N_4. However, a further increase in the temperature beyond 650 °C resulted in a blue shift of optical absorption, which was ascribed to the quantum confinement effect. Thus, the right choice of temperature and synthesis condition is key to selectively promoting n → π* transition, that can red-shift the optical absorption.

The effect of thermal exfoliation on the optical absorption was studied by Yang et al.[130] Partial destruction of the in-plane H-bonding was induced by thermal exfoliation of pristine g-C_3N_4, resulting in the formation of ultrathin g-C_3N_4 nanosheets. The modified g-C_3N_4 was found to have a distorted layered structure because of the outward movement of the amino groups, eventually resulting in the outward twisting of the melon units. An additional absorption observed around 450−550 nm may be due to n → π* transitions due to partial loss of planarity in g-C_3N_4. These low-energy photons were indeed capable of H_2 evolution, evidenced by wavelength-dependent studies.

In addition to the two methods discussed in this section, using chemical reagents such as oxamide enabled n → π* transitions by inducing planar asymmetry in g-C_3N_4.[131] This resulted in an additional absorption around 520 nm, which was effectively utilized to realize H_2 evolution. Collectively, it can be inferred that post-calcination thermal treatment under a specific gaseous atmosphere is an effective route to red-shift the optical absorption beyond 460 nm, originating from the pronounced n → π* transition as indicated by T_2 in Figure 12. Extended absorption was achieved by inducing partial/marginal loss of structural planarity in g-C_3N_4, promoting electron transitions at lower energy (λ > 460 nm). Table 4 lists various routes to induce structural distortions in g-C_3N_4 and its

https://doi.org/10.1021/acsanm.3c04740
ACS Appl. Nano Mater. 2023, 6, 19551−19572

Table 5. Various Reports Evidencing N-Vacancy Induced Red-Shift in Optical Absorption and the Resulting Improvement in Photocatalytic H_2 Evolution Efficiency

Precursor	Method to induce N-vacancies	Bandgap (eV)		H_2 evolution rate		Ref.
		Before	After	Before	After	
Melamine	Post-calcination thermal treatment under H_2 atmosphere	2.78	2.76	3.67 μmol h^{-1}	64.39 μmol h^{-1}	132
Dicyandiamide	Thermal polymerization under H_2 atmosphere	≈2.75	2.0	≈1 μmol g^{-1}	≈6 μmol g^{-1}	133
Urea	Postcalcination $NaBH_4$ thermal treatment	3.01	2.97	481.6 μmol g^{-1} h^{-1}	8171.4 μmol g^{-1} h^{-1}	134
Dicyandiamide	Hydrothermal treatment followed by two-step calcination	2.84	2.60	374.7 μmol g^{-1} h^{-1}	3259.1 μmol g^{-1} h^{-1}	135

effect on the optical band gap and photocatalytic H_2 evolution efficiency.

4.4. Inducing N-Vacancies below π^* (LUMO). Another way to extend the optical absorption is by deliberately creating N-vacancies below π^* orbitals. Generally, post-synthesis treatment of g-C_3N_4 can result in stoichiometric imbalance, leading to some loss of N atoms in g-C_3N_4, resulting in the formation of unoccupied energy levels referred to as N-vacancies below the π^* orbitals. The formation of N-vacancies is expected to increase the C/N ratio in g-C_3N_4. Electron transitions are now possible from π orbitals to N-vacancies at lower energy (T_2 in Figure 13) than the fundamental transition (T_1 in Figure 13). Therefore, creating N-vacancies in g-C_3N_4 can potentially red-shift the optical absorption.

Formation of N-vacancies was achieved by post-calcination thermal treatment under H_2 environment.[132] This method induced the loss of two-coordinated N-atoms (N1 in Figure 7), thereby creating N-vacancies, red-shifting the optical absorption to 600 nm due to T_2 transition (Figure 13). Furthermore, the low-energy photons (λ > 460 nm) were found to be active for photocatalytic CO_2 reduction and the H_2 production. Similarly, heating melon in H_2 atmosphere induced N-vacancies, which red-shifted the optical absorption up to 850 nm.[136] In addition to post-synthesis thermal treatment, synthesizing g-C_3N_4 in the H_2 environment also resulted in the loss of N1-atoms, forming N-vacancies, which resulted in substantial red-shift of optical absorption up to 700 nm.[133] Such changes in the structural and optoelectronic properties enhanced the photocatalytic efficiency of H_2 evolution[133] and rhodamine B degradation.[136]

Employing chemical reductants such as $N_2H_4{\cdot}H_2O$,[134] which decomposes to form reductive gases like NH_3 and H_2, further facilitated the N-vacancies formation. The loss of two-coordinated N-atoms (N1 in Figure 7) was preferred over the loss of three-coordinated N-atoms (N2, N3, and N4 in Figure 7). Introducing N-vacancies extended light absorption up to 600 nm and promoted charge separation/transfer efficiency, collectively improving the photocatalytic H_2 evolution efficiency by 26 times. In another approach, hydrothermal synthesis of melamine and triethanol amine (TEOA) followed by calcination formed ultrathin g-C_3N_4 nanosheets.[137] Addition of TEOA led to an increase in the pyridinic N (N1 in Figure 7) and decreased the presence of graphitic N (N3 in Figure 7). This loss of some of the graphitic N indicated the presence of N-vacancies and substantially red-shifted the optical absorption to 800 nm and exhibited wavelength-dependent H_2 evolution up to 550 nm. Table 5 lists selected reports that demonstrated enhanced photocatalytic H_2 evolution efficiency on introducing N-vacancies.

Note that methods to introduce N-vacancies can also result in partial distortion of structural integrity, which also red-shifts the optical absorption. Therefore, differentiating the nature of electron transitions (HOMO to unoccupied N-vacancies or n $\rightarrow \pi^*$ orbitals) responsible for the red-shifting the absorption in these two categories is rather complex. Further investigation in this direction is necessary. Nevertheless, this approach demonstrated red-shifted absorption and also pronounced photocatalytic H_2 generation.

4.5. Doping. The doping of foreign elements into the g-C_3N_4 host has been found to induce changes in the optical absorption, consequently affecting the photocatalytic performance.[138] This section is subdivided into metal and non-metal doping.

4.5.1. Non-metal Doping. C-doping (also referred as self-doping) of g-C_3N_4 is a promising and facile approach to controlling the optoelectronic properties. This method has substantially red-shifted optical absorption toward the NIR region,[139] attributed to the extended π-delocalized network due to C-doping at the bridging nitrogen site (N4 in Figure 7) of g-C_3N_4. In addition, C-doping was found to improve the electrical conductivity by 2 orders of magnitude.[140] C-doping has enhanced the overall photocatalytic performance toward H_2 evolution,[140] dye degradation,[141] and NO removal.[139]

Among different methods for C-doping, the supramolecular assembly approach has recently gained prominent attention. Mondal et al. controlled the structural ordering and solubility of the melamine-based precursors via supramolecular assembly using a water-ethylene glycol mixture.[142] This method of C-doping red-shifted the optical absorption and demonstrated photocatalytic H_2 evolution efficiency using low-energy photons up to 595 nm. In another study, supramolecular interaction between terephthalic acid and melamine induced via H-bonding formed a network of carbon-rich-conjugated cocrystals.[143] On thermal polymerization of such cocrystals, graphitic carbon offering extended conjugated network was incorporated into g-C_3N_4 (evidenced by increased C to N ratio). Concurrently, the optical absorption was remarkably extended to 800 nm. Such carbon-rich g-C_3N_4 also promoted efficient charge transport, enhancing the photocatalytic overall water splitting reaction.

Porous C-doped g-C_3N_4 was synthesized via gas-bubbles induced thermal exfoliation method[144] using acrylamide (as a template reagent) with dicyandiamide. This method resulted g-C_3N_4 with extended optical absorption up to 800 nm. The newly formed −C═C− bond (confirmed from XPS analysis) due to C-doping offers enhanced electron delocalization, concurrently leading to a pronounced $\pi \rightarrow \pi^*$ transition. Furthermore, wavelength-dependent H_2 evolution data supported the efficient utilization of low-energy photons (λ > 460 nm).

O-doped g-C_3N_4 was successfully synthesized via the solvothermal method using dicyandiamide and 1,3,5-trichlorotriazine as C- and N-rich precursors.[145] The latter was prone to oxidation when exposed to air and is the origin of O-doping. Oxygen was found to replace sp^2-N (N1 in Figure 7) and concurrently red-shifted the optical absorption to 750 nm.

https://doi.org/10.1021/acsanm.3c04740
ACS Appl. Nano Mater. 2023, 6, 19551−19572

Table 6. Various Reports Evidencing Non-metal Dopant-Induced Red-Shift of Optical Absorption and Subsequently Improved Photocatalytic H_2 Generation Efficiency

Dopant	Synthesis process	Bandgap (eV)		H_2 evolution rate		Ref.
		Before	After	Before	After	
C	Gaseous bubble template method	2.78	2.23	372.5 μmol g^{-1} h^{-1}	1266.8 μmol g^{-1} h^{-1}	144
S	Hydrothermal treatment followed by calcination	2.72	2.71	4 mmol g^{-1} h^{-1}	22.04 mmol g^{-1} h^{-1}	148
P	Supramolecular thermal polymerization	2.74	2.65	10.4 μmol h^{-1}	256.4 μmol h^{-1}	149
B	Microwave heating method	-	-	613 μmol g^{-1} h^{-1}	1439 μmol g^{-1} h^{-1}	150
Br	Thermal polymerization	2.86	2.82	20 μmol h^{-1}	48 μmol h^{-1}	151
I	Thermal polymerization	2.75	2.70	14 μmol h^{-1}	38 μmol h^{-1}	152
B, P	Thermal polymerization	2.90	2.80	≈0.75 mmol g^{-1} h^{-1}	4.0 mmol g^{-1} h^{-1}	153
C	Thermal annealing condensation	2.76	2.44	≈400 μmol	≈1700 μmol	154
O	Solvothermal method	2.73	2.21	846 μmol g^{-1} h^{-1}	3174 μmol g^{-1} h^{-1}	145
S	Thermal polymerization	2.80	2.59	67.9 μmol g^{-1} h^{-1}	525.5 μmol g^{-1} h^{-1}	155

Such extended absorption can be attributed to the increased electron density in HOMO due to O-doping. In another work, thermal oxidation-exfoliation of bulk g-C_3N_4 formed nanosheets, which upon further curling condensation resulted in porous O-doped g-C_3N_4 nanotubes (OCN-tube).[146] Such OCN-tube was found to form −C≡N and −C−O−C− (confirmed by XPS and FTIR), which red-shifted absorption to 500 nm. DFT studies indicate that the −C≡N functional group induces HOMO−LUMO redistribution, resulting in a reduced band gap.[147]

Thiourea oxide was employed as the dopant's source to synthesize S-, O-doped g-C_3N_4.[138] Oxygen substituted for two-coordinated N atom (N1, refer Figure 7) of the g-C_3N_4, whereas S was vertically bonded to the carbon atom. Replacing N of g-C_3N_4 by O may likely create N-related vacancies below the LUMO in g-C_3N_4, promoting electron transition from $\pi \rightarrow$ N-vacancies at lower energy (λ > 460 nm). These features collectively extended the absorption toward 690 nm in S-, O-doped g-C_3N_4.

Guo et al. investigated the effect of doping an electron-deficient (B) and electron-rich atom (S) on the optical property of g-C_3N_4.[156] Boron doping is expected to draw the electron density from its surrounding π-plane conjugate system, which is likely the reason for the blue-shift of optical absorption. In contrast, S-doping red-shifted the absorption to 480 nm, attributed to increased electron density in the π-conjugation system. In addition, the lone pair of electrons in S can elicit optical transition to π^* orbitals, resulting in red-shifted optical absorption (460 to 700 nm).[155] Similarly, S-doped poly(heptazine imide) prepared via supramolecular preassembly of melamine and trithiocyanuric acid also red-shifted the absorption.[157] Thus, S-doping successfully enhanced the photocatalytic H_2 generation efficiency using low-energy photons (λ < 550 nm). In another method for S-doping, hydrothermal treatment of precursors with sulfuric acid significantly red-shifted the absorption to the NIR region and also enhanced photocatalytic CO_2 reduction.[158]

There is no conclusive correlation between the doping of g-C_3N_4 with halogens and the resulting optical properties. For example, Zhang et al. reported that iodine doping of g-C_3N_4 red-shifted the optical absorption to 650 nm owing to the formation of donor levels above the HOMO. However, doping F, Cl, and Br did not yield any significant effect on the optical absorption of g-C_3N_4.[152] A number of mutually correlated factors like the dopant's size, substitution site and the electronegativity of the dopant could play a key role here. Further investigation in this direction is required. Nevertheless, doping of several non-metals red-shifted the optical absorption and also promoted photocatalytic H_2 evolution efficiency (λ > 460 nm). Such results are listed in Table 6.

4.5.2. Metal Doping. In addition to non-metal, metal doping is expected to alter the optoelectronic property of g-C_3N_4. Cation is incorporated by coordinating with nitrogen atoms (N1 in Figure 7) of g-C_3N_4. The change in the electronic structure of g-C_3N_4 depends on the extent of charge transfer between metal and the ligand in g-C_3N_4.

Among various alkali metals (Li^+, Na^+, K^+, Rb^+) doped to g-C_3N_4, Rb exhibited a maximum red-shift of optical absorption until 600 nm and also demonstrated enhanced photocatalytic CO_2 reduction.[159] The computational analysis predicts C atoms of the tri-s-triazine as likely sites for doping alkali metals. However, experimental evidence to support this notion is missing. Wang et al. extended the optical absorption of g-C_3N_4 toward 540 nm by polymerizing melamine with KCl, followed by post-modification.[160] This K-doped g-C_3N_4 demonstrated a factor 30 increment in the H_2 evolution activity compared to pristine g-C_3N_4 (synthesized via thermal polymerization of melamine without KCl). Another route to synthesize K-doped g-C_3N_4 was by treating the as-synthesized g-C_3N_4 in KOH, followed by calcination.[161] K^+ replaced the H atom bonded to the N atom (N2 in Figure 7) of terminal amino groups. Despite decreasing the crystallinity of g-C_3N_4, K-doping extended the absorption toward 520 nm. A similar red-shift of optical absorption was observed on doping alkaline earth metals as well.[162]

Similar to alkali and alkali earth metals, doping transition metal cations are also found to significantly red-shift the optical absorption. For example, Cu doping promoted the coordination between Cu and N (N1 in Figure 7), concurrently red-shifting the optical absorption toward 480 nm.[163] However, the observed 30 times enhancement in H_2 evolution efficiency compared to undoped g-C_3N_4 was attributed to improved charge separation and charge transfer efficiency upon Cu doping. Ce-doping of g-C_3N_4 via a pyrolysis approach introduced multivalent Ce ions (+3 and +4).[164] In this case, Ce-ion is substituted for bridging N atoms (N4 in Figure 7) of g-C_3N_4. However, the extent of red-shift in the optical absorption was less than 20 nm. In another case, extended absorption to $\lambda \geq$ 520 nm upon Ni-doping of g-C_3N_4 was attributed to the charge transfer transition between Ni 3d orbitals and N 2p orbitals.[165,166] A similar charge transfer mechanism from Zn 3d orbitals to N 2p orbitals of g-C_3N_4 red-shifted the optical absorption to 600 nm in Zn-doped g-C_3N_4.[167] In addition, the low energy photons (540 nm) were

https://doi.org/10.1021/acsanm.3c04740
ACS Appl. Nano Mater. 2023, 6, 19551−19572

Table 7. Various Reports Evidencing Metal-Dopant Induced Red-Shift of Optical Absorption and Subsequently Improved Photocatalytic H_2 Generation Efficiency in g-C_3N_4

Dopant	Synthesis process	Bandgap (eV)		H_2 evolution rate		Ref.
		Before	After	Before	After	
Pd	Thermal condensation	-	-	25 μmol g^{-1}	316.2 μmol g^{-1}	171
Zn	Soft-chemical method followed by thermal polymerization	-	-	5.5 μmol h^{-1}	59.5 μmol h^{-1}	167
Ni	One-step pyrolysis	2.73	2.61	98.67 μmol g^{-1} h^{-1}	155.71 μmol g^{-1} h^{-1}	166
K	Vapor-deposition method	2.80	2.50	0.059 mmol g^{-1} h^{-1}	1.948 mmol g^{-1} h^{-1}	160
Co	Thermal polymerization	2.70	2.62	9.5 μmol h^{-1}	28.0 μmol h^{-1}	172

effectively utilized for reducing protons to generate H_2. In the case of Fe-doped g-C_3N_4, coordination of Fe with sp^2-N (N1 in Figure 7) of the tri-s-triazine ring may lead to partial transfer of lone pair of electrons from electron-rich g-C_3N_4 ring to Fe^{3+}.[168] Such effect was found to reduce the band gap to 2.48 eV.[169] Though Fe doping did not distort the structural integrity of g-C_3N_4, observing a substantial decrease in PL intensity was attributed to the electron-trapping nature of Fe^{3+} states.

Li et al. realized NIR absorption in g-C_3N_4 by Pt incorporation due to the metal-to-ligand charge transfer (MLCT) excited state formation.[170] The electron-rich N-pots (voids) surrounded by two coordinated N atoms (N1 in Figure 7) consisting of six lone pair of electrons was found to be the site of Pt^{2+} inclusion. Computational analysis revealed the formation of metal−ligand hybrid HOMO via strong coordination of Pt^{2+} with the N-pots. Such MLCT interaction resulted in extreme red-shifting of the absorption onset toward 1100 nm. In addition, such low-energy photon absorption successfully promoted electrons to LUMO and was effectively utilized to generate H_2. This work evidenced how a strategic synthesis approach can offer optoelectronic tunability in g-C_3N_4 to realize NIR absorption.

Despite significant studies, the origin of red-shifted optical absorption in metal-doped g-C_3N_4 is unclear. It is due to an inadequate understanding of the electronic nature of interaction/bonding between the metal cations and the g-C_3N_4 framework. In some cases, metal-doped g-C_3N_4 resulted in virtually no change in the optical absorption.[173−179] A comprehensive correlation between the nature of the dopant and the resulting structural/surface/optoelectronic properties is yet to be established. Table 7 lists selected metal-doped g-C_3N_4 evidencing doping-induced extended absorption and enhanced photocatalytic H_2 generation efficiency.

4.6. Interplay between C/N Ratio. In stoichiometrically perfect g-C_3N_4, the C/N ratio is 0.75, which is seldom achieved. However, there are efforts to modulate the C/N ratio from 0.75, which has led to the emergence of two subcategories of carbon nitrides, namely carbon subnitrides (C/N > 0.75) and carbon supernitrides (C/N < 0.75).

Thermal treatment of melem hydrazine resulted in the formation of carbon supernitride (C_3N_5).[180] C_3N_5 was found to have a significantly low band gap (1.76 eV) due to the nitrogen-rich matrix. The red-shift in optical absorption was attributed to the extended conjugation owing to the orbital overlap of N of the azo group as well as the N of the heptazine rings. In addition, the electrons of residual amine groups also contributed to the π-conjugation, upshifting the HOMO leading to a reduced band gap. A hard template-assisted method was employed for the synthesis of C_3N_5, having a reduced band gap of 2.2 eV.[181] The presence of triazoles in C_3N_5 led to strong π-conjugation, significantly red-shifting the optical absorption. These electron transitions beyond 460 nm furnished free electrons in the LUMO, which led to superior H_2 evolution under visible light irradiation in comparison to so far reported g-C_3N_4 photocatalysts. On the other hand, an extensive network of π-conjugation systems in carbon subnitride (C_2N) resulted in an extremely low band gap of 1.96 eV.[182] However, further studies regarding utilizing this material for suitable photocatalytic reactions are yet to be undertaken. Therefore, it can be inferred that the extreme deviation of the C/N ratio from the ideal 0.75 value significantly reduces the band gap. Moreover, the extent of conjugation and electron density is significantly increased by achieving extreme C/N ratios in these two materials (subnitrides and supernitrides), effectively red-shifted their optical absorption.

The topics discussed so far highlight various synthesis approaches which can red-shift the optical absorption of g-C_3N_4. While improving the efficiency and extent of light absorption remains critical, the overall photocatalytic efficiency is collectively determined by the efficiency of charge generation and charge separation. The efficiency of the latter two processes is studied by investigating the fundamental photophysical loss processes in g-C_3N_4. Figure 14 presents the

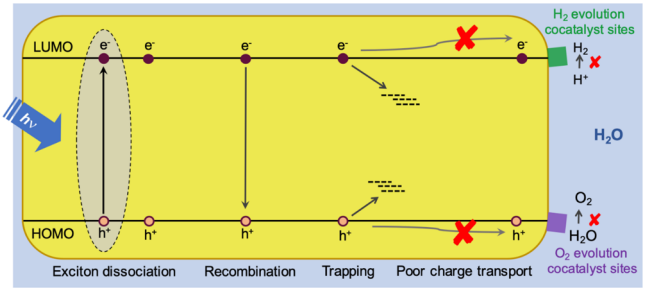

Figure 14. Summary of photophysical processes limiting the efficiency of photocatalytic water splitting reaction in g-C_3N_4. Upon light absorption, the generated excitons undergo subsequent dissociation to form free charge carriers, which further decay via recombination and/or trapping, leading to inadequate number of charge carriers reaching the interface for photocatalytic redox reactions.

fundamental loss processes that limit the photocatalytic performance of g-C_3N_4. As per the current understanding,[183−185] it is unclear whether photoexcitation of g-C_3N_4 generates free charge carriers or excitons, or a mixture of both. Earlier reports addressing this question are not conclusive. For example, an ultrafast transient absorption spectroscopy (TAS) study by Godin et al. found no evidence to support the exciton formation in g-C_3N_4. However, in another work by Corp et al. the monomolecular fluence-independent decay of photoluminescence signal suggests excitonic behavior.[184] However, TAS measurement of the same sample shows fluence-

https://doi.org/10.1021/acsanm.3c04740
ACS Appl. Nano Mater. 2023, 6, 19551−19572

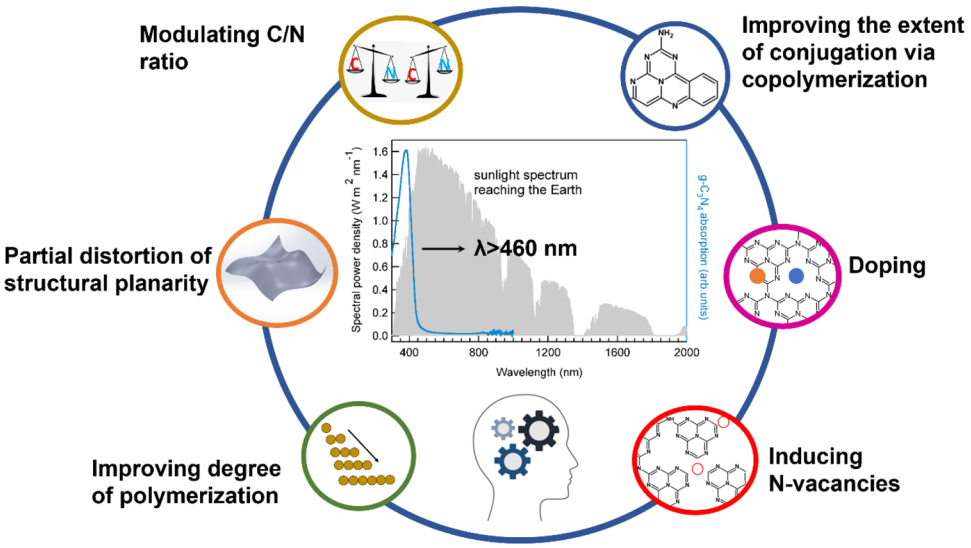

Figure 15. A summary of various approaches to red-shift the optical absorption of g-C_3N_4 to enhance the photocatalytic efficiency.

dependent decay behavior, which can be explained by considering bimolecular type recombination of free charge carriers. Based on these observations, it is amenable that photoexcitation of g-C_3N_4 generates both excitons and free carriers. Corp et al. estimated the upper limit of charge separation efficiency as 65% in g-C_3N_4.[184] It indicates the possibility of further enhancing the free carrier generation yield via exciton dissociation efficiency, which otherwise decays via recombination to the ground state results in a loss process.

The photogenerated charge carriers in the bulk must migrate to the surface of g-C_3N_4 to be successfully involved in the charge transfer reaction. However, the concurrent charge carrier trapping and electron hole recombination is in kinetic competition with the charge transfer process. In this direction, Tong et al. demonstrated how improving the crystallinity of g-C_3N_4 reduces the recombination rate and promotes the efficiency of the key electron transfer process, which enhanced the H_2 generation efficiency.[186] Similarly, Godin et al. attributed charge carrier trapping as the major reason limiting the photocatalytic H_2 generation efficiency.[183]

These loss processes discussed here reduce the number of photogenerated charge carriers that can reach the interface, consequently limiting the photocatalytic performance. Thus, it is essential to establish a correlation between charge generation efficiency, recombination and trapping with synthesis conditions. Obtaining such mechanistic insight to effectively utilize all the photogenerated carriers is equally important as extending the light absorption to achieve higher STH energy conversion efficiency of g-C_3N_4.

5. CONCLUSIONS AND OUTLOOK

Figure 15 depicts various approaches to red-shift the optical absorption of g-C_3N_4 that are discussed in this Review. The synthesis procedures, precursors, and dopants incorporated have a significant role in tuning the electronic structure of g-C_3N_4. In this section, we critically review the effectiveness of all the six methods identified for extending the optical absorption and utilizing λ > 460 nm photons for photocatalytic H_2 evolution.

5.1. Improving the Degree of Polymerization. While increasing the degree of polymerization has a definite impact on the optical absorption due to pronounced $\pi \rightarrow \pi^*$, this results in only a considerable decrease in the band gap. Additionally, expecting light absorption beyond 480 nm in g-C_3N_4 modified via this approach is unrealistic. Hence, there exists limited or no reports evidencing wavelength-dependent photocatalytic performance.

5.2. Extending the Degree of Conjugation via Copolymerization. Copolymerization results in the incorporation of aromatic and/or organic comonomers in the tri-s-triazine rings, which extends the conjugation. This approach has significantly red-shifted the optical absorption of g-C_3N_4 to as long as 700 nm. Note that wavelength-dependent H_2 evolution reaction is demonstrated in several reports, which reinforces the success rate of this approach. Additionally, copolymerization is a bottom-up approach, and hence, it offers immense opportunity to choose desirable precursors to incorporate aromatic entities in the tri-s-triazine ring. With such prospects, copolymerization is a promising approach to improve the light absorption efficiency of the g-C_3N_4 photocatalysts.

5.3. Enabling n $\rightarrow$ π^* Transition. As discussed in detail, structural distortion of g-C_3N_4 planarity to enable n $\rightarrow$ π^* transitions has significantly red-shifted the optical absorption (λ<600 nm). While some groups have employed post-calcination thermal treatment to introduce structural distortion, using chemical reagents to realize the same effect is also reported. Thermal exfoliation of pristine g-C_3N_4 has also been reported to promote n $\rightarrow$ π^* transitions. Therefore, generalizing the synthesis approach in this case is not possible. Nonetheless, wavelength-dependent H_2 evolution data in low-energy (λ > 460 nm) demonstrates the utility of this approach to drive photocatalytic reactions. To further get insights into this approach, establishing a comprehensive correlation between the synthesis parameter, resulting optoelectronic properties, and wavelength-dependent photocatalytic performance is essential.

5.4. Inducing N-Vacancies. Unoccupied N-vacancies below LUMO were induced by chemical reductants and controlled thermal treatment during and post-synthesis. While the formation of unoccupied states was attributed to the loss of two-coordinated N atom (N1 in Figure 7), there exists limited insight into the stability of such systems upon vacancy formation. Additionally, due to their energetic position, the

https://doi.org/10.1021/acsanm.3c04740
ACS Appl. Nano Mater. 2023, 6, 19551−19572

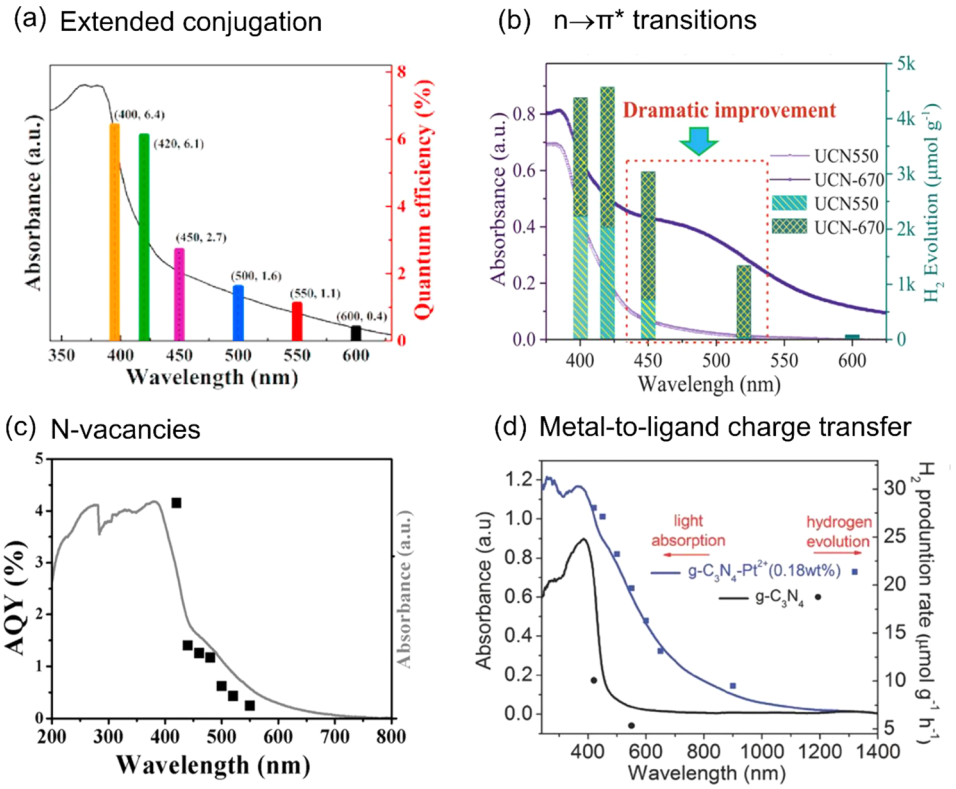

Figure 16. Wavelength-dependent photocatalytic H_2 evolution evidenced by various modified g-C_3N_4 photocatalysts. (a) g-C_3N_4 copolymerized with *N*-phenylthiourea. Reproduced from ref 108. Copyright 2021 Elsevier. (b) g-C_3N_4 without (UCN550) and with (UCN670) partial distortion. Reproduced with permission from ref 129. Copyright 2021 John Wiley and Sons. (c) g-C_3N_4 with N-vacancies. Reproduced from ref 132. Copyright 2022 American Chemical Society. (d) Pristine g-C_3N_4 and g-C_3N_4-Pt^{2+}, the latter exhibiting H_2 evolution even at 900 nm. Reproduced with permission from ref 170. Copyright 2016 John Wiley and Sons.

electrons in these levels may not have the required thermodynamic energy to drive specific reactions, like H_2 evolution. The post-calcination thermal treatment has induced N-vacancies in some cases while enabling n → π^* transitions in a few cases. Hence, attributing the red shift of optical absorption to a specific set of electron transitions is complex and necessitates detailed investigation.

5.5. Doping. By introducing a foreign element into the host g-C_3N_4, an electronic redistribution may lead to a reduced band gap. There exist numerous reports on metal and non-metal doped g-C_3N_4, but very few reports justify the observed doping-induced changes in the optical properties. Considering a specific non-metallic element (phosphorus), for instance, conflicting reports exists evidencing red-shift,[149] blue-shift[187] and virtually no shift[188] of the optical absorption. Such observation can be linked to the synthesis approach and detailed insight into such observations is required. Nonetheless, doping S, C and O has indeed red-shifted the light absorption by increasing the electron density. Various synthesis approaches discussed in non-metal doping introduced atoms or heteroatoms within the g-C_3N_4 network, exhibiting red-shift of optical absorption. On the other hand, there are several reports where synthesis or modification approaches introduced functional groups such as carboxylic and hydroxyl groups in the carbon nitride network. While introducing polar functional groups improved the water-dispersibility of the samples, it blue-shifted the optical absorption.[189−191]

On the other hand, metal doping of g-C_3N_4 red-shifted the optical absorption, which was primarily attributed to the charge transfer between metal and tri-s-triazine unit of g-C_3N_4 acting as the ligand. However, wavelength-dependent studies evidencing the successful use of λ>460 nm photons to drive photocatalytic activity were demonstrated in very few reports in both the categories, i.e., metal and nonmetal doping.

5.6. Modulating C/N Ratio. Synthesizing carbon nitrides with extreme C/N ratios has demonstrated to substantially improve the light absorption efficiency. There are very few reports in this area. With the available data, it can be deduced that N-rich matrix of carbon nitrides have reduced band gaps simultaneously evidencing wavelength-dependent H_2 evolution. On the other hand, a band gap as low as 1.96 eV was achieved by synthesizing carbon-rich matrix (C_2N).[182] However, to the best of our understanding, photocatalytic H_2 evolution activity reports are not yet available for such materials. However, in achieving such extreme C/N ratios, the graphitic structure of carbon nitride is significantly compromised. Hence, these materials have structures and optoelectronic properties that significantly differ from those of g-C_3N_4.

Note that merely extending the spectral response of g-C_3N_4 to the visible/NIR region does not always enhance the photocatalytic performance. It is essential to consider the nature of electronic transitions and where electrons are eventually promoted due to light absorption. Figure 16 presents several reports that effectively utilize these low energy photons (λ > 460 nm) for H_2 generation. It also demonstrates wavelength-dependent H_2 evolution at λ > 460 nm. The key to utilizing low-energy photons for photocatalytic reaction lies in understanding the interplay between the synthesis parameters and the nature of optical transitions that contribute to red-

https://doi.org/10.1021/acsanm.3c04740
ACS Appl. Nano Mater. 2023, 6, 19551−19572

shifting the absorption of g-C_3N_4. Such insights are essential to enhancing the solar energy conversion efficiency of g-C_3N_4.

While g-C_3N_4 offers tunable optoelectronic properties, this is primarily limited to powder samples. The direct fabrication of the g-C_3N_4 thin film electrodes is challenging and is one of the factors limiting its wide applications to optoelectronics. Typically, g-C_3N_4 in powder form is coated on the conducting substrates via disperse coating, doctor blade method, or drop casting. While these methods are simple, they do not ensure good electrical contact between the substrate and the sample.[192,193] Alternatively, fabricating electrodes by particle transfer method is successful in several classes of photocatalytic materials.[194−197] However, this approach is yet to be explored for fabricating g-C_3N_4 electrodes. Nonetheless, g-C_3N_4 thin films were successfully produced on different substrates (Si and glass) through the CVD technique, showing the promise toward electrode fabrication.[69] Further research in the direct fabrication of g-C_3N_4 thin films with extended optical absorption opens up several opportunities in optoelectronics and photocatalytic/photoelectrochemical reactions.

AUTHOR INFORMATION

Corresponding Author

Dharmapura H. K. Murthy − *Department of Chemistry, Manipal Institute of Technology and Centre for Renewable Energy, Manipal Institute of Technology, Manipal Academy of Higher Education, Manipal, Karnataka, India 576104;* orcid.org/0000-0003-3462-7269; Email: murthy.dharmapura@manipal.edu

Authors

Sujana Chandrappa − *Department of Chemistry, Manipal Institute of Technology, Manipal Academy of Higher Education, Manipal, Karnataka, India 576104*

Simon Joyson Galbao − *Department of Chemistry, Manipal Institute of Technology, Manipal Academy of Higher Education, Manipal, Karnataka, India 576104;* orcid.org/0000-0002-1724-3311

Akihiro Furube − *Institute of Post-LED Photonics, Tokushima University, Tokushima 770-8506, Japan;* orcid.org/0000-0002-4682-0843

Complete contact information is available at: https://pubs.acs.org/10.1021/acsanm.3c04740

Notes

The authors declare no competing financial interest.

ACKNOWLEDGMENTS

D.H.K.M. acknowledges Technology Mission Division (Energy, Water & All Others), Department of Science & Technology (DST), Ministry of Science & Technology, Government of India, reference number DST/TMD/IC-MAP/2K20/02, project titled as Integrated Clean Energy Material Acceleration Platform (IC-MAP) on bioenergy and hydrogen. S.C. thanks DST, Government of India, for the Junior Research Fellowship.

REFERENCES

(1) Lewis, N. S. Toward Cost-Effective Solar Energy Use. *Science* **2007**, *315* (5813), 798−801.

(2) Fassioli, F.; Dinshaw, R.; Arpin, P. C.; Scholes, G. D. Photosynthetic Light Harvesting: Excitons and Coherence. *J. R. Soc. Interface* **2014**, *11* (92), 20130901.

(3) Wang, Y.; Suzuki, H.; Xie, J.; Tomita, O.; Martin, D. J.; Higashi, M.; Kong, D.; Abe, R.; Tang, J. Mimicking Natural Photosynthesis: Solar to Renewable H_2 Fuel Synthesis by Z-Scheme Water Splitting Systems. *Chem. Rev.* **2018**, *118* (10), 5201−5241.

(4) Nguyen, P. D.; Duong, T. M.; Tran, P. D. Current Progress and Challenges in Engineering Viable Artificial Leaf for Solar Water Splitting. *J. Sci. Adv. Mater. Devices* **2017**, *2* (4), 399−417.

(5) Fujishima, A.; Honda, K. Electrochemical Photolysis of Water at a Semiconductor Electrode. *Nature* **1972**, *238* (5358), 37−38.

(6) Iizuka, K.; Wato, T.; Miseki, Y.; Saito, K.; Kudo, A. Photocatalytic Reduction of Carbon Dioxide over Ag Cocatalyst-Loaded $ALa_4Ti_4O_{15}$ (A = Ca, Sr, and Ba) Using Water as a Reducing Reagent. *J. Am. Chem. Soc.* **2011**, *133* (51), 20863−20868.

(7) Zhang, S.; He, Z.; Li, X.; Zhang, J.; Zang, Q.; Wang, S. Building Heterogeneous Nanostructures for Photocatalytic Ammonia Decomposition. *Nanoscale Adv.* **2020**, *2* (9), 3610−3623.

(8) Obata, K.; Kishishita, K.; Okemoto, A.; Taniya, K.; Ichihashi, Y.; Nishiyama, S. Photocatalytic Decomposition of NH_3 over TiO_2 Catalysts Doped with Fe. *Appl. Catal. B Environ.* **2014**, *160−161*, 200−203.

(9) Navakoteswara Rao, V.; Lakshmana Reddy, N.; Mamatha Kumari, M.; Ravi, P.; Sathish, M.; Kuruvilla, K. M.; Preethi, V.; Reddy, K. R.; Shetti, N. P.; Aminabhavi, T. M.; Shankar, M. V. Photocatalytic Recovery of H_2 from H_2S Containing Wastewater: Surface and Interface Control of Photo-Excitons in Cu_2S@TiO_2 Core-Shell Nanostructures. *Appl. Catal. B Environ.* **2019**, *254*, 174−185.

(10) Uekert, T.; Kasap, H.; Reisner, E. Photoreforming of Nonrecyclable Plastic Waste over a Carbon Nitride/Nickel Phosphide Catalyst. *J. Am. Chem. Soc.* **2019**, *141* (38), 15201−15210.

(11) Uekert, T.; Pichler, C. M.; Schubert, T.; Reisner, E. Solar-Driven Reforming of Solid Waste for a Sustainable Future. *Nat. Sustain.* **2021**, *4* (5), 383−391.

(12) Ahmad, K.; Ghatak, H. R.; Ahuja, S. M. A Review on Photocatalytic Remediation of Environmental Pollutants and H_2 Production through Water Splitting: A Sustainable Approach. *Environ. Technol. Innov.* **2020**, *19*, No. 100893.

(13) Ong, W.-J.; Tan, L.-L.; Ng, Y. H.; Yong, S.-T.; Chai, S.-P. Graphitic Carbon Nitride (g-C_3N_4)-Based Photocatalysts for Artificial Photosynthesis and Environmental Remediation: Are We a Step Closer To Achieving Sustainability? *Chem. Rev.* **2016**, *116* (12), 7159−7329.

(14) Kamat, P. V.; Christians, J. A. Solar Cells versus Solar Fuels: Two Different Outcomes. *J. Phys. Chem. Lett.* **2015**, *6* (10), 1917−1918.

(15) Nishiyama, H.; Yamada, T.; Nakabayashi, M.; Maehara, Y.; Yamaguchi, M.; Kuromiya, Y.; Nagatsuma, Y.; Tokudome, H.; Akiyama, S.; Watanabe, T.; Narushima, R.; Okunaka, S.; Shibata, N.; Takata, T.; Hisatomi, T.; Domen, K. Photocatalytic Solar Hydrogen Production from Water on a 100-m^2 Scale. *Nature* **2021**, *598* (7880), 304−307.

(16) Zhou, P.; Navid, I. A.; Ma, Y.; Xiao, Y.; Wang, P.; Ye, Z.; Zhou, B.; Sun, K.; Mi, Z. Solar-to-Hydrogen Efficiency of More than 9% in Photocatalytic Water Splitting. *Nature* **2023**, *613* (7942), 66−70.

(17) Iwase, A.; Yoshino, S.; Takayama, T.; Ng, Y. H.; Amal, R.; Kudo, A. Water Splitting and CO_2 Reduction under Visible Light Irradiation Using Z-Scheme Systems Consisting of Metal Sulfides, CoO_x-Loaded $BiVO_4$, and a Reduced Graphene Oxide Electron Mediator. *J. Am. Chem. Soc.* **2016**, *138* (32), 10260−10264.

(18) Yoshino, S.; Sato, K.; Yamaguchi, Y.; Iwase, A.; Kudo, A. Z-Schematic CO_2 Reduction to CO through Interparticle Electron Transfer between $SrTiO_3$:Rh of a Reducing Photocatalyst and $BiVO_4$ of a Water Oxidation Photocatalyst under Visible Light. *ACS Appl. Energy Mater.* **2020**, *3* (10), 10001−10007.

(19) Suzuki, T. M.; Yoshino, S.; Takayama, T.; Iwase, A.; Kudo, A.; Morikawa, T. Z-Schematic and Visible-Light-Driven CO_2 Reduction Using H_2O as an Electron Donor by a Particulate Mixture of a Ru-Complex/$(CuGa)_{1-x}Zn_{2x}S_2$ Hybrid Catalyst, $BiVO_4$ and an Electron Mediator. *Chem. Commun.* **2018**, *54* (72), 10199−10202.

(20) Saravanan, R.; Gracia, F.; Stephen, A. *Basic Principles, Mechanism, and Challenges of Photocatalysis*; 2017; pp 19−40. DOI: 10.1007/978-3-319-62446-4_2.
(21) Yang, X.; Wang, D. Photocatalysis: From Fundamental Principles to Materials and Applications. *ACS Appl. Energy Mater.* **2018**, *1* (12), 6657−6693.
(22) Murthy, D. H. K.; Matsuzaki, H.; Liu, J.; Suzuki, Y.; Hisatomi, T.; Seki, K.; Domen, K.; Furube, A. Transient Absorption Spectroscopy Reveals Performance-Limiting Factors in a Narrow-Bandgap Oxysulfide $La_5(Ti_{0.99}Mg_{0.01})_2CuS_5O_{6.99}$ Photocatalyst for H_2 Generation. *J. Phys. Chem. C* **2019**, *123* (23), 14246−14252.
(23) Murthy, D. H. K.; Nandal, V.; Furube, A.; Seki, K.; Katoh, R.; Lyu, H.; Hisatomi, T.; Domen, K.; Matsuzaki, H. Origin of Enhanced Overall Water Splitting Efficiency in Aluminum-Doped $SrTiO_3$ Photocatalyst. *Adv. Energy Mater.* **2023**, No. 2302064.
(24) Ohtani, B. Photocatalysis A to Z—What We Know and What We Do Not Know in a Scientific Sense. *J. Photochem. Photobiol. C Photochem. Rev.* **2010**, *11* (4), 157−178.
(25) Banerjee, S.; Pillai, S. C.; Falaras, P.; O'Shea, K. E.; Byrne, J. A.; Dionysiou, D. D. New Insights into the Mechanism of Visible Light Photocatalysis. *J. Phys. Chem. Lett.* **2014**, *5* (15), 2543−2554.
(26) Liu, B.; Wu, H.; Parkin, I. P. New Insights into the Fundamental Principle of Semiconductor Photocatalysis. *ACS Omega* **2020**, *5* (24), 14847−14856.
(27) Schneider, J.; Matsuoka, M.; Takeuchi, M.; Zhang, J.; Horiuchi, Y.; Anpo, M.; Bahnemann, D. W. Understanding TiO_2 Photocatalysis: Mechanisms and Materials. *Chem. Rev.* **2014**, *114* (19), 9919−9986.
(28) Ong, C. B.; Ng, L. Y.; Mohammad, A. W. A Review of ZnO Nanoparticles as Solar Photocatalysts: Synthesis, Mechanisms and Applications. *Renew. Sustain. Energy Rev.* **2018**, *81*, 536−551.
(29) Pastor, E.; Sachs, M.; Selim, S.; Durrant, J. R.; Bakulin, A. A.; Walsh, A. Electronic Defects in Metal Oxide Photocatalysts. *Nat. Rev. Mater.* **2022**, *7* (7), 503−521.
(30) Khan, M. M.; Adil, S. F.; Al-Mayouf, A. Metal Oxides as Photocatalysts. *J. Saudi Chem. Soc.* **2015**, *19* (5), 462−464.
(31) Kumar, A.; Kumar, A.; Krishnan, V. Perovskite Oxide Based Materials for Energy and Environment-Oriented Photocatalysis. *ACS Catal.* **2020**, *10* (17), 10253−10315.
(32) Irshad, M.; Ain, Q. t.; Zaman, M.; Aslam, M. Z.; Kousar, N.; Asim, M.; Rafique, M.; Siraj, K.; Tabish, A. N.; Usman, M.; Hassan Farooq, M. u.; Assiri, M. A.; Imran, M. Photocatalysis and Perovskite Oxide-Based Materials: A Remedy for a Clean and Sustainable Future. *RSC Adv.* **2022**, *12* (12), 7009−7039.
(33) Fagan, R.; McCormack, D. E.; Dionysiou, D. D.; Pillai, S. C. A Review of Solar and Visible Light Active TiO_2 Photocatalysis for Treating Bacteria, Cyanotoxins and Contaminants of Emerging Concern. *Mater. Sci. Semicond. Process.* **2016**, *42*, 2−14.
(34) Wang, Z.; Liu, Y.; Huang, B.; Dai, Y.; Lou, Z.; Wang, G.; Zhang, X.; Qin, X. Progress on Extending the Light Absorption Spectra of Photocatalysts. *Phys. Chem. Chem. Phys.* **2014**, *16* (7), 2758.
(35) Malato-Rodríguez, S. Solar Detoxification and Disinfection. In *Encyclopedia of Energy*; Elsevier, 2004; pp 587−596. DOI: 10.1016/B0-12-176480-X/00323-5.
(36) Ellis, A. B.; Kaiser, S. W.; Bolts, J. M.; Wrighton, M. S. Study of N-Type Semiconducting Cadmium Chalcogenide-Based Photoelectrochemical Cells Employing Polychalcogenide Electrolytes. *J. Am. Chem. Soc.* **1977**, *99* (9), 2839−2848.
(37) Sato, K.; Fujii, K.; Koike, K.; Goto, T.; Yao, T. Anomalous Time Variation of Photocurrent in GaN during Photoelectrochemical Reaction for H_2 Gas Generation in NaOH Aqueous Solution. *Phys. Status Solidi C* **2009**, *6* (S2), S635−S638.
(38) Edalati, P.; Shen, X.-F.; Watanabe, M.; Ishihara, T.; Arita, M.; Fuji, M.; Edalati, K. High-Entropy Oxynitride as a Low-Bandgap and Stable Photocatalyst for Hydrogen Production. *J. Mater. Chem. A* **2021**, *9* (26), 15076−15086.
(39) Li, C.; Xu, Y.; Tu, W.; Chen, G.; Xu, R. Metal-Free Photocatalysts for Various Applications in Energy Conversion and Environmental Purification. *Green Chem.* **2017**, *19* (4), 882−899.
(40) Rahman, M. Z.; Kibria, M. G.; Mullins, C. B. Metal-Free Photocatalysts for Hydrogen Evolution. *Chem. Soc. Rev.* **2020**, *49* (6), 1887−1931.
(41) Fujita, S.; Habuchi, H.; Takagi, S.; Takikawa, H. Optical Properties of Graphitic Carbon Nitride Films Prepared by Evaporation. *Diam. Relat. Mater.* **2016**, *65*, 83−86.
(42) Cook, S.; Furube, A.; Katoh, R. Analysis of the Excited States of Regioregular Polythiophene P3HT. *Energy Environ. Sci.* **2008**, *1* (2), 294.
(43) Wang, X.; Maeda, K.; Thomas, A.; Takanabe, K.; Xin, G.; Carlsson, J. M.; Domen, K.; Antonietti, M. A Metal-Free Polymeric Photocatalyst for Hydrogen Production from Water under Visible Light. *Nat. Mater.* **2009**, *8* (1), 76−80.
(44) Liang, J.; Yang, X.; Wang, Y.; He, P.; Fu, H.; Zhao, Y.; Zou, Q.; An, X. A Review on g-C_3N_4 Incorporated with Organics for Enhanced Photocatalytic Water Splitting. *J. Mater. Chem. A* **2021**, *9* (22), 12898−12922.
(45) Zhang, G.; Lan, Z.-A.; Lin, L.; Lin, S.; Wang, X. Overall Water Splitting by Pt/g-C_3N_4 Photocatalysts without Using Sacrificial Agents. *Chem. Sci.* **2016**, *7* (5), 3062−3066.
(46) Aggarwal, M.; Basu, S.; Shetti, N. P.; Nadagouda, M. N.; Kwon, E. E.; Park, Y.-K.; Aminabhavi, T. M. Photocatalytic Carbon Dioxide Reduction: Exploring the Role of Ultrathin 2D Graphitic Carbon Nitride (g-C_3N_4). *Chem. Eng. J.* **2021**, *425*, No. 131402.
(47) Liu, R.; Chen, Z.; Yao, Y.; Li, Y.; Cheema, W. A.; Wang, D.; Zhu, S. Recent Advancements in g-C_3N_4-Based Photocatalysts for Photocatalytic CO_2 Reduction: A Mini Review. *RSC Adv.* **2020**, *10* (49), 29408−29418.
(48) Yang, X.; Zhang, L.; Wang, D.; Zhang, Q.; Zeng, J.; Zhang, R. Facile Synthesis of Nitrogen-Defective g-C_3N_4 for Superior Photocatalytic Degradation of Rhodamine B. *RSC Adv.* **2021**, *11* (49), 30503−30509.
(49) Samanta, S.; Srivastava, R. Graphitic Carbon Nitride for Organic Transformation. In *Nanoscale Graphitic Carbon Nitride*; Elsevier, 2022; pp 393−456. DOI: 10.1016/B978-0-12-823034-3.00012-1.
(50) Yang, Q.; Pan, G.; Wei, J.; Wang, W.; Tang, Y.; Cai, Y. Remarkable Activity of Potassium-Modified Carbon Nitride for Heterogeneous Photocatalytic Decarboxylative Alkyl/Acyl Radical Addition and Reductive Dimerization of Para -Quinone Methides. *ACS Sustain. Chem. Eng.* **2021**, *9* (5), 2367−2377.
(51) Geng, P.; Tang, Y.; Pan, G.; Wang, W.; Hu, J.; Cai, Y. A g-C_3N_4 -Based Heterogeneous Photocatalyst for Visible Light Mediated Aerobic Benzylic C−H Oxygenations. *Green Chem.* **2019**, *21* (22), 6116−6122.
(52) Zhu, Q.; Zhang, J. Is g-C_3N_4 More Suitable for Photocatalytic Reduction or Oxidation in Environmental Applications? *Environ. Funct. Mater.* **2022**, *1* (1), 121−125.
(53) Zheng, Q.; Xu, E.; Park, E.; Chen, H.; Shuai, D. Looking at the Overlooked Hole Oxidation: Photocatalytic Transformation of Organic Contaminants on Graphitic Carbon Nitride under Visible Light Irradiation. *Appl. Catal. B Environ.* **2019**, *240*, 262−269.
(54) Song, Z.; Li, Z.; Lin, L.; Zhang, Y.; Lin, T.; Chen, L.; Cai, Z.; Lin, S.; Guo, L.; Fu, F.; Wang, X. Phenyl-Doped Graphitic Carbon Nitride: Photoluminescence Mechanism and Latent Fingerprint Imaging. *Nanoscale* **2017**, *9* (45), 17737−17742.
(55) Barrio, J.; Barzilai, S.; Karjule, N.; Amo-Ochoa, P.; Zamora, F.; Shalom, M. Fluorescent Carbon Nitride Macrostructures Derived from Triazine-Based Cocrystals. *Adv. Opt. Mater.* **2021**, *9* (19), 2100683.
(56) Ghosh, A.; Saini, H.; Sarkar, A.; Guha, P.; Samantara, A. K.; Thapa, R.; Mandal, S.; Mandal, A.; Behera, J. N.; Ray, S. K.; Goswami, D. K. Nitrogen Vacancy and Hydrogen Substitution Mediated Tunable Optoelectronic Properties of g-C_3N_4 2D Layered Structures: Applications towards Blue LED to Broad-Band Photodetection. *Appl. Surf. Sci.* **2021**, *556*, No. 149773.
(57) Das, D.; Shinde, S. L.; Nanda, K. K. Temperature-Dependent Photoluminescence of g-C_3N_4: Implication for Temperature Sensing. *ACS Appl. Mater. Interfaces* **2016**, *8* (3), 2181−2186.

(58) Schröder, M.; Kailasam, K.; Borgmeyer, J.; Neumann, M.; Thomas, A.; Schomäcker, R.; Schwarze, M. Hydrogen Evolution Reaction in a Large-Scale Reactor Using a Carbon Nitride Photocatalyst under Natural Sunlight Irradiation. *Energy Technol.* **2015**, *3* (10), 1014−1017.
(59) Maeda, K.; Domen, K. Photocatalytic Water Splitting: Recent Progress and Future Challenges. *J. Phys. Chem. Lett.* **2010**, *1* (18), 2655−2661.
(60) van Benthem, K.; Elsässer, C.; French, R. H. Bulk Electronic Structure of $SrTiO_3$: Experiment and Theory. *J. Appl. Phys.* **2001**, *90* (12), 6156−6164.
(61) Teter, D. M.; Hemley, R. J. Low-Compressibility Carbon Nitrides. *Science.* **1996**, *271* (5245), 53−55.
(62) Molina, B.; Sansores, L. E. Electronic Structure of Six Phases of C_3N_4: A Theoretical Approach. *Mod. Phys. Lett. B* **1999**, *13* (06n07), 193−201.
(63) Döblinger, M.; Lotsch, B. V.; Wack, J.; Thun, J.; Senker, J.; Schnick, W. Structure Elucidation of Polyheptazine Imide by Electron Diffraction—a Templated 2D Carbon Nitride Network. *Chem. Commun.* **2009**, 1541−1543.
(64) Chang, M.; Pan, Z.; Zheng, D.; Wang, S.; Zhang, G.; Anpo, M.; Wang, X. Salt-Melt Synthesis of Poly Heptazine Imides with Enhanced Optical Absorption for Photocatalytic Hydrogen Production. *ChemSusChem* **2023**, *16* (13), e202202255.
(65) Wirnhier, E.; Döblinger, M.; Gunzelmann, D.; Senker, J.; Lotsch, B. V.; Schnick, W. Poly(Triazine Imide) with Intercalation of Lithium and Chloride Ions $[(C_3N_3)_2(NH_xLi_{1-x})_3{\cdot}LiCl]$: A Crystalline 2D Carbon Nitride Network. *Chem. − Eur. J.* **2011**, *17* (11), 3213−3221.
(66) Yan, S. C.; Li, Z. S.; Zou, Z. G. Photodegradation Performance of g-C_3N_4 Fabricated by Directly Heating Melamine. *Langmuir* **2009**, *25* (17), 10397−10401.
(67) Zhang, Y.; Liu, J.; Wu, G.; Chen, W. Porous Graphitic Carbon Nitride Synthesized via Direct Polymerization of Urea for Efficient Sunlight-Driven Photocatalytic Hydrogen Production. *Nanoscale* **2012**, *4* (17), 5300.
(68) Xin, G.; Meng, Y. Pyrolysis Synthesized g-C_3N_4 for Photocatalytic Degradation of Methylene Blue. *J. Chem.* **2013**, *2013*, 1−5.
(69) Chubenko, E. B.; Kovalchuk, N. G.; Komissarov, I. V.; Borisenko, V. E. Chemical Vapor Deposition of 2D Crystallized g-C_3N_4 Layered Films. *J. Phys. Chem. C* **2022**, *126* (9), 4710−4714.
(70) Giusto, P.; Cruz, D.; Heil, T.; Arazoe, H.; Lova, P.; Aida, T.; Comoretto, D.; Patrini, M.; Antonietti, M. Shine Bright Like a Diamond: New Light on an Old Polymeric Semiconductor. *Adv. Mater.* **2020**, *32* (10), 1908140.
(71) Chen, L.; Yan, R.; Oschatz, M.; Jiang, L.; Antonietti, M.; Xiao, K. Ultrathin 2D Graphitic Carbon Nitride on Metal Films: Underpotential Sodium Deposition in Adlayers for Sodium-Ion Batteries. *Angew. Chemie Int. Ed.* **2020**, *59* (23), 9067−9073.
(72) Hu, C.; Chu, Y.-C.; Wang, M.-S.; Wu, X.-H. Rapid Synthesis of g-C_3N_4 Spheres Using Microwave-Assisted Solvothermal Method for Enhanced Photocatalytic Activity. *J. Photochem. Photobiol. A Chem.* **2017**, *348*, 8−17.
(73) Hu, C.-C.; Wang, M.-S.; Hung, W.-Z. Influence of Solvothermal Synthesis on the Photocatalytic Degradation Activity of Carbon Nitride under Visible Light Irradiation. *Chem. Eng. Sci.* **2017**, *167*, 1−9.
(74) Gago, R.; Jiménez, I.; Cáceres, D.; Agulló-Rueda, F.; Sajavaara, T.; Albella, J. M.; Climent-Font, A.; Vergara, I.; Räisänen, J.; Rauhala, E. Hardening Mechanisms in Graphitic Carbon Nitride Films Grown with N_2 /Ar Ion Assistance. *Chem. Mater.* **2001**, *13* (1), 129−135.
(75) Tang, W.; Tian, Y.; Chen, B.; Xu, Y.; Li, B.; Jing, X.; Zhang, J.; Xu, S. Supramolecular Copolymerization Strategy for Realizing the Broadband White Light Luminescence Based on N-Deficient Porous Graphitic Carbon Nitride (g-C_3N). *ACS Appl. Mater. Interfaces* **2020**, *12* (5), 6396−6406.
(76) Zhao, C.; Ding, C.; Han, C.; Yang, X.; Xu, J. Lignin-Incorporated Supramolecular Copolymerization Yielding g-C_3N_4 Nanoarchitectures for Efficient Photocatalytic Hydrogen Evolution. *Sol. RRL* **2021**, *5* (2), 200486.
(77) Wen, Y.; Qu, D.; An, L.; Gao, X.; Jiang, W.; Wu, D.; Yang, D.; Sun, Z. Defective g-C $_3N_4$ Prepared by the $NaBH_4$ Reduction for High-Performance H_2 Production. *ACS Sustain. Chem. Eng.* **2019**, *7* (2), 2343−2349.
(78) Guo, S.; Zhang, H.; Yang, P.; Chen, Y.; Yu, X.; Yu, B.; Zhao, Y.; Yang, Z.; Liu, Z. Visible-Light-Driven Photoreduction of CO_2 to CO over Porous Nitrogen-Deficient Carbon Nitride Nanotubes. *Catal. Sci. Technol.* **2019**, *9* (10), 2485−2492.
(79) Hu, Y.; Shim, Y.; Oh, J.; Park, S.; Park, S.; Ishii, Y. Synthesis of ^{13}C-, ^{15}N-Labeled Graphitic Carbon Nitrides and NMR-Based Evidence of Hydrogen-Bonding Assisted Two-Dimensional Assembly. *Chem. Mater.* **2017**, *29* (12), 5080−5089.
(80) Wang, C.; Xiao, H.; Lu, Y.; Lv, J.; Yuan, Z.; Cheng, J. Regulation of Polymerization Kinetics to Improve Crystallinity of Carbon Nitride for Photocatalytic Reactions. *ChemSusChem* **2023**, *16* (16), No. e202300361.
(81) Jiang, J.; Ou-yang, L.; Zhu, L.; Zheng, A.; Zou, J.; Yi, X.; Tang, H. Dependence of Electronic Structure of g-C_3N_4 on the Layer Number of Its Nanosheets: A Study by Raman Spectroscopy Coupled with First-Principles Calculations. *Carbon N. Y.* **2014**, *80*, 213−221.
(82) Ismael, M.; Wu, Y. A Mini-Review on the Synthesis and Structural Modification of g-C_3N_4-Based Materials, and Their Applications in Solar Energy Conversion and Environmental Remediation. *Sustain. Energy Fuels* **2019**, *3* (11), 2907−2925.
(83) Wang, A.; Wang, C.; Fu, L.; Wong-Ng, W.; Lan, Y. Recent Advances of Graphitic Carbon Nitride-Based Structures and Applications in Catalyst, Sensing, Imaging, and LEDs. *Nano-Micro Lett.* **2017**, *9* (4), 47.
(84) Jürgens, B.; Irran, E.; Senker, J.; Kroll, P.; Müller, H.; Schnick, W. Melem (2,5,8-Triamino-Tri- s -Triazine), an Important Intermediate during Condensation of Melamine Rings to Graphitic Carbon Nitride: Synthesis, Structure Determination by X-Ray Powder Diffractometry, Solid-State NMR, and Theoretical Studies. *J. Am. Chem. Soc.* **2003**, *125* (34), 10288−10300.
(85) Zhang, G.; Zhang, J.; Zhang, M.; Wang, X. Polycondensation of Thiourea into Carbon Nitride Semiconductors as Visible Light Photocatalysts. *J. Mater. Chem.* **2012**, *22* (16), 8083.
(86) Sharma, P.; Sarngan, P. P.; Lakshmanan, A.; Sarkar, D. One-Step Synthesis of Highly Reactive g-C_3N_4. *J. Mater. Sci. Mater. Electron.* **2022**, *33* (12), 9116−9125.
(87) Wang, Y.; Di, Y.; Antonietti, M.; Li, H.; Chen, X.; Wang, X. Excellent Visible-Light Photocatalysis of Fluorinated Polymeric Carbon Nitride Solids. *Chem. Mater.* **2010**, *22* (18), 5119−5121.
(88) Bojdys, M. J.; Müller, J.-O.; Antonietti, M.; Thomas, A. Ionothermal Synthesis of Crystalline, Condensed, Graphitic Carbon Nitride. *Chem. - A Eur. J.* **2008**, *14* (27), 8177−8182.
(89) Sattler, A.; Pagano, S.; Zeuner, M.; Zurawski, A.; Gunzelmann, D.; Senker, J.; Müller-Buschbaum, K.; Schnick, W. Melamine-Melem Adduct Phases: Investigating the Thermal Condensation of Melamine. *Chem. - A Eur. J.* **2009**, *15* (47), 13161−13170.
(90) Lotsch, B. V.; Schnick, W. From Triazines to Heptazines: Novel Nonmetal Tricyanomelaminates as Precursors for Graphitic Carbon Nitride Materials. *Chem. Mater.* **2006**, *18* (7), 1891−1900.
(91) Hoppe, H.; Sariciftci, N. S. Nanostructure and Nanomorphology Engineering in Polymer Solar Cells. In *Nanostructured Materials for Solar Energy Conversion*; Elsevier, 2006; pp 277−318. DOI: 10.1016/B978-044452844-5/50011-1.
(92) Chen, Y.; Wang, B.; Lin, S.; Zhang, Y.; Wang, X. Activation of n → Π* Transitions in Two-Dimensional Conjugated Polymers for Visible Light Photocatalysis. *J. Phys. Chem. C* **2014**, *118* (51), 29981−29989.
(93) Lee, S. Y.; Lee, G.; Jun, Y.-S.; Park, Y. Il. Visible/near-Infrared Driven Highly Efficient Photocatalyst Based on Upconversion Nanoparticles/g-C_3N_4 Nanocomposite. *Appl. Surf. Sci.* **2020**, *508*, No. 144839.

(94) Liu, Y.; Ma, Z. g-C_3N_4 Modified by Meso-Tetrahydroxyphenylchlorin for Photocatalytic Hydrogen Evolution Under Visible/Near-Infrared Light. *Front. Chem.* **2020**, *8*, 605343.
(95) Feng, L.; He, F.; Liu, B.; Yang, G.; Gai, S.; Yang, P.; Li, C.; Dai, Y.; Lv, R.; Lin, J. g-C_3N_4 Coated Upconversion Nanoparticles for 808 Nm Near-Infrared Light Triggered Phototherapy and Multiple Imaging. *Chem. Mater.* **2016**, *28* (21), 7935−7946.
(96) Ullah, I.; Ling, C.; Li, J.-H.; Lu, X.-J.; Yang, Z.; Wang, G.; Xu, A.-W. Metallic TiN Nanoparticles Loaded on g-C_3N_4 for Plasmon Enhanced Visible and NIR Photocatalytic H_2 Evolution from Water Splitting. *Inorg. Chem. Front.* **2023**, *10* (11), 3326−3334.
(97) Zhao, F.; Khaing, K. K.; Yin, D.; Liu, B.; Chen, T.; Wu, C.; Huang, K.; Deng, L.; Li, L. Large Enhanced Photocatalytic Activity of g-C_3N_4 by Fabrication of a Nanocomposite with Introducing Upconversion Nanocrystal and Ag Nanoparticles. *RSC Adv.* **2018**, *8* (74), 42308−42321.
(98) Liu, N.; Li, T.; Zhao, Z.; Liu, J.; Luo, X.; Yuan, X.; Luo, K.; He, J.; Yu, D.; Zhao, Y. From Triazine to Heptazine: Origin of Graphitic Carbon Nitride as a Photocatalyst. *ACS Omega* **2020**, *5* (21), 12557−12567.
(99) Wang, Y.; Zhang, Y.; Li, B.; Luo, K.; Shi, K.; Zhang, L.; Li, Y.; Yu, T.; Hu, W.; Xie, C.; Wu, Y.; Su, L.; Dong, X.; Zhao, Z.; Yang, G. Restacked Melon as Highly-Efficient Photocatalyst. *Nano Energy* **2020**, *77*, No. 105124.
(100) Hong, Y.; Fang, Z.; Yin, B.; Luo, B.; Zhao, Y.; Shi, W.; Li, C. A Visible-Light-Driven Heterojunction for Enhanced Photocatalytic Water Splitting over Ta_2O_5 Modified g-C_3N_4 Photocatalyst. *Int. J. Hydrogen Energy* **2017**, *42* (10), 6738−6745.
(101) Bian, J.; Li, J.; Kalytchuk, S.; Wang, Y.; Li, Q.; Lau, T. C.; Niehaus, T. A.; Rogach, A. L.; Zhang, R.-Q. Efficient Emission Facilitated by Multiple Energy Level Transitions in Uniform Graphitic Carbon Nitride Films Deposited by Thermal Vapor Condensation. *ChemPhysChem* **2015**, *16* (5), 954−959.
(102) Mo, Z.; She, X.; Li, Y.; Liu, L.; Huang, L.; Chen, Z.; Zhang, Q.; Xu, H.; Li, H. Synthesis of g-C_3N_4 at Different Temperatures for Superior Visible/UV Photocatalytic Performance and Photoelectrochemical Sensing of MB Solution. *RSC Adv.* **2015**, *5* (123), 101552−101562.
(103) Zhang, M.; Wang, X. Two Dimensional Conjugated Polymers with Enhanced Optical Absorption and Charge Separation for Photocatalytic Hydrogen Evolution. *Energy Environ. Sci.* **2014**, *7* (6), 1902−1906.
(104) Piercy, V. L.; Neri, G.; Manning, T. D.; Pugliese, A.; Blanc, F.; Palgrave, R. G.; Cowan, A. J.; Rosseinsky, M. J. Band Structure Engineering of Carbon Nitride Hybrid Photocatalysts for CO_2 Reduction in Aqueous Solutions. *J. Mater. Chem. A* **2023**, *11* (34), 18356−18364.
(105) Zhang, J.; Chen, X.; Takanabe, K.; Maeda, K.; Domen, K.; Epping, J. D.; Fu, X.; Antonietti, M.; Wang, X. Synthesis of a Carbon Nitride Structure for Visible-Light Catalysis by Copolymerization. *Angew. Chemie Int. Ed.* **2010**, *49* (2), 441−444.
(106) Shibata, K.; Kato, K.; Tsounis, C.; Kanazawa, T.; Lu, D.; Nozawa, S.; Yamakata, A.; Ishitani, O.; Maeda, K. Synthesis of Copolymerized Carbon Nitride Nanosheets from Urea and 2-Aminobenzonitrile for Enhanced Visible Light CO_2 Reduction with a Ruthenium(II) Complex Catalyst. *Sol. RRL* **2020**, *4* (8), 1900461.
(107) Zhang, J.; Zhang, G.; Chen, X.; Lin, S.; Möhlmann, L.; Dołęga, G.; Lipner, G.; Antonietti, M.; Blechert, S.; Wang, X. Co-Monomer Control of Carbon Nitride Semiconductors to Optimize Hydrogen Evolution with Visible Light. *Angew. Chemie Int. Ed.* **2012**, *51* (13), 3183−3187.
(108) Jiang, R.; Lu, G.; Liu, J.; Wu, D.; Yan, Z.; Wang, Y. Incorporation of π-Conjugated Molecules as Electron Donors in g-C_3N_4 Enhances Photocatalytic H_2-Production. *Renew. Energy* **2021**, *164*, 531−540.
(109) Chen, Y.; Zhang, J.; Zhang, M.; Wang, X. Molecular and Textural Engineering of Conjugated Carbon Nitride Catalysts for Selective Oxidation of Alcohols with Visible Light. *Chem. Sci.* **2013**, *4* (8), 3244.
(110) Zhang, J.; Zhang, M.; Lin, S.; Fu, X.; Wang, X. Molecular Doping of Carbon Nitride Photocatalysts with Tunable Bandgap and Enhanced Activity. *J. Catal.* **2014**, *310*, 24−30.
(111) Xu, C.; Liu, X.; Li, D.; Chen, Z.; Yang, J.; Huang, J.; Pan, H. Coordination of π-Delocalization in g-C_3N_4 for Efficient Photocatalytic Hydrogen Evolution under Visible Light. *ACS Appl. Mater. Interfaces* **2021**, *13* (17), 20114−20124.
(112) Li, Y.; Jin, R.; Li, G.; Liu, X.; Yu, M.; Xing, Y.; Shi, Z. Preparation of Phenyl Group Functionalized g-C_3N_4 Nanosheets with Extended Electron Delocalization for Enhanced Visible-Light Photocatalytic Activity. *New J. Chem.* **2018**, *42* (9), 6756−6762.
(113) Guan, H.; Zhang, W. Delocalization of Π-Electron in Graphitic Carbon Nitride to Promote Its Photocatalytic Activity for Hydrogen Evolution. *ChemCatChem.* **2019**, *11* (22), 5633−5641.
(114) Karjule, N.; Barrio, J.; Tzadikov, J.; Shalom, M. Electronic Structure Engineering of Carbon Nitride Materials by Using Polycyclic Aromatic Hydrocarbons. *Chem. − Eur. J.* **2020**, *26* (29), 6622−6628.
(115) Li, K.; Sun, M.; Zhang, W.-D. Polycyclic Aromatic Compounds-Modified Graphitic Carbon Nitride for Efficient Visible-Light-Driven Hydrogen Evolution. *Carbon N. Y.* **2018**, *134*, 134−144.
(116) Wu, X.; Fan, H.; Wang, W.; Lei, L.; Chang, X.; Ma, L. Multiple Ordered Porous Honeycombed g-C_3N_4 with Carbon Ring In-Plane Splicing for Outstanding Photocatalytic H_2 Production. *J. Mater. Chem. A* **2022**, *10*, 17817.
(117) Xia, Z.; Li, Y.; Yang, Q.; Zhu, W.; Jin, R.; Zhang, L.; Xing, Y. Electron-Induced Effect and Coordinated Pi-Delocalization Synergistically Promote Charge Transfer in Benzenesulfonic Acid Modified g-C_3N_4 with Efficient Photocatalytic Performance. *Catal. Sci. Technol.* **2022**, *12* (21), 6599−6608.
(118) Gao, S.; Wan, S.; Yu, J.; Cao, S. Donor−Acceptor Modification of Carbon Nitride for Enhanced Photocatalytic Hydrogen Evolution. *Adv. Sustain. Syst.* **2023**, *7* (1), 2200130.
(119) Chen, X.; Xu, Y.; Xu, G. Modification of Graphite Carbon Nitride by Adding an Ultra-Micro Amount of Triaminotriphenylamine for Superior Photocatalytic Hydrogen Evolution. *New J. Chem.* **2022**, *46* (19), 9057−9063.
(120) Jin, X.; Zhang, L.; Fan, X.; Tian, J.; Wang, M.; Shi, J. A photo-excited electron transfer hyperchannel constructed in P. pyrimidine-modified carbon nitride for remarkably enhanced water-splitting photocatalytic activity; Zhang, L.; Fan, X.; Tian, J.; Wang, M.; Shi, J. A Photo-Excited Electron Transfer Hyperchannel Constructed in Pt-Dispersed Pyrimidine-Modified Carbon Nitride for Remarkably Enhanced Water-Splitting Photocatalytic Activity. *Appl. Catal. B Environ.* **2018**, *237*, 888−894.
(121) Wu, X.; Fan, H.; Wang, W.; Lei, L.; Chang, X.; Ma, L. Multiple Ordered Porous Honeycombed g-C_3N_4 with Carbon Ring in-Plane Splicing for Outstanding Photocatalytic H_2 Production. *J. Mater. Chem. A* **2022**, *10* (34), 17817−17826.
(122) Cheng, C.; Mao, L.; Huang, Z.; Shi, J.; Zheng, B.; Zhang, Y.; Guo, L. Bridging Regulation in Graphitic Carbon Nitride for Band-Structure Modulation and Directional Charge Transfer towards Efficient H_2 Evolution under Visible-Light Irradiation. *J. Colloid Interface Sci.* **2021**, *601*, 220−228.
(123) Jorge, A. B.; Martin, D. J.; Dhanoa, M. T. S.; Rahman, A. S.; Makwana, N.; Tang, J.; Sella, A.; Corà, F.; Firth, S.; Darr, J. A.; McMillan, P. F. H_2 and O_2 Evolution from Water Half-Splitting Reactions by Graphitic Carbon Nitride Materials. *J. Phys. Chem. C* **2013**, *117* (14), 7178−7185.
(124) Deifallah, M.; McMillan, P. F.; Corà, F. Electronic and Structural Properties of Two-Dimensional Carbon Nitride Graphenes. *J. Phys. Chem. C* **2008**, *112* (14), 5447−5453.
(125) Ho, W.; Zhang, Z.; Xu, M.; Zhang, X.; Wang, X.; Huang, Y. Enhanced Visible-Light-Driven Photocatalytic Removal of NO: Effect on Layer Distortion on g-C_3N_4 by H_2 Heating. *Appl. Catal. B Environ.* **2015**, *179*, 106−112.
(126) Hu, S.; Jiang, D.; Gu, L.; Xu, G.; Li, Z.; Yuan, Y. Awakening n → Π* Electronic Transition by Breaking Hydrogen Bonds in

Graphitic Carbon Nitride for Increased Photocatalytic Hydrogen Generation. *Chem. Eng. J.* **2020**, *399*, No. 125847.
(127) Dias, E. M.; Christoforidis, K. C.; Francàs, L.; Petit, C. Tuning Thermally Treated Graphitic Carbon Nitride for H_2 Evolution and CO_2 Photoreduction: The Effects of Material Properties and Mid-Gap States. *ACS Appl. Energy Mater.* **2018**, *1* (11), 6524−6534.
(128) Zhou, C.; Zeng, G.; Huang, D.; Luo, Y.; Cheng, M.; Liu, Y.; Xiong, W.; Yang, Y.; Song, B.; Wang, W.; Shao, B.; Li, Z. Distorted Polymeric Carbon Nitride via Carriers Transfer Bridges with Superior Photocatalytic Activity for Organic Pollutants Oxidation and Hydrogen Production under Visible Light. *J. Hazard. Mater.* **2020**, *386*, No. 121947.
(129) An, S.; Zhang, G.; Li, K.; Huang, Z.; Wang, X.; Guo, Y.; Hou, J.; Song, C.; Guo, X. Self-Supporting 3D Carbon Nitride with Tunable n → Π* Electronic Transition for Enhanced Solar Hydrogen Production. *Adv. Mater.* **2021**, *33* (49), 2104361.
(130) Yang, Y.; Chen, J.; Mao, Z.; An, N.; Wang, D.; Fahlman, B. D. Ultrathin g-C_3N_4 Nanosheets with an Extended Visible-Light-Responsive Range for Significant Enhancement of Photocatalysis. *RSC Adv.* **2017**, *7* (4), 2333−2341.
(131) Zhang, G.; Savateev, A.; Zhao, Y.; Li, L.; Antonietti, M. Advancing the n → Π* Electron Transition of Carbon Nitride Nanotubes for H_2 Photosynthesis. *J. Mater. Chem. A* **2017**, *5* (25), 12723−12728.
(132) Tu, W.; Xu, Y.; Wang, J.; Zhang, B.; Zhou, T.; Yin, S.; Wu, S.; Li, C.; Huang, Y.; Zhou, Y.; Zou, Z.; Robertson, J.; Kraft, M.; Xu, R. Investigating the Role of Tunable Nitrogen Vacancies in Graphitic Carbon Nitride Nanosheets for Efficient Visible-Light-Driven H_2 Evolution and CO_2 Reduction. *ACS Sustain. Chem. Eng.* **2017**, *5* (8), 7260−7268.
(133) Tay, Q.; Kanhere, P.; Ng, C. F.; Chen, S.; Chakraborty, S.; Huan, A. C. H.; Sum, T. C.; Ahuja, R.; Chen, Z. Defect Engineered g-C_3N_4 for Efficient Visible Light Photocatalytic Hydrogen Production. *Chem. Mater.* **2015**, *27* (14), 4930−4933.
(134) Wu, J.; Li, N.; Fang, H.-B.; Li, X.; Zheng, Y.-Z.; Tao, X. Nitrogen Vacancies Modified Graphitic Carbon Nitride: Scalable and One-Step Fabrication with Efficient Visible-Light-Driven Hydrogen Evolution. *Chem. Eng. J.* **2019**, *358*, 20−29.
(135) Liao, Y.; Wang, G.; Wang, J.; Wang, K.; Yan, S.; Su, Y. Nitrogen Vacancy Induced in Situ g-C_3N_4 p-n Homojunction for Boosting Visible Light-Driven Hydrogen Evolution. *J. Colloid Interface Sci.* **2021**, *587*, 110−120.
(136) Niu, P.; Yin, L.-C.; Yang, Y.-Q.; Liu, G.; Cheng, H.-M. Increasing the Visible Light Absorption of Graphitic Carbon Nitride (Melon) Photocatalysts by Homogeneous Self-Modification with Nitrogen Vacancies. *Adv. Mater.* **2014**, *26* (47), 8046−8052.
(137) Yang, M.; Duan, R.; Mei, J.; Yang, B.; Yang, H.; Sun, S.; Liang, S.; Cui, J. Fabricating Transfer Channel and Charge Trap in Carbon Nitride Ultrathin Nanosheet for Enhanced Photocatalytic Hydrogen Evolution. *Int. J. Hydrogen Energy* **2023**, *48* (26), 9690−9699.
(138) Yuan, S.; Zhang, Q.; Xu, B.; Liu, S.; Wang, J.; Xie, J.; Zhang, M.; Ohno, T. A New Precursor to Synthesize g-C_3N_4 with Superior Visible Light Absorption for Photocatalytic Application. *Catal. Sci. Technol.* **2017**, *7* (9), 1826−1830.
(139) Zhao, Z.; Sun, Y.; Dong, F.; Zhang, Y.; Zhao, H. Template Synthesis of Carbon Self-Doped g-C_3N_4 with Enhanced Visible to near-Infrared Absorption and Photocatalytic Performance. *RSC Adv.* **2015**, *5* (49), 39549−39556.
(140) Barrio, J.; Lin, L.; Amo-Ochoa, P.; Tzadikov, J.; Peng, G.; Sun, J.; Zamora, F.; Wang, X.; Shalom, M. Unprecedented Centimeter-Long Carbon Nitride Needles: Synthesis, Characterization and Applications. *Small* **2018**, *14* (21), No. 1800633.
(141) Dong, G.; Zhao, K.; Zhang, L. Carbon Self-Doping Induced High Electronic Conductivity and Photoreactivity of g-C_3N_4. *Chem. Commun.* **2012**, *48* (49), 6178.
(142) Mondal, S.; Mark, G.; Abisdris, L.; Li, J.; Shmila, T.; Tzadikov, J.; Volokh, M.; Xing, L.; Shalom, M. Developing Extended Visible Light Responsive Polymeric Carbon Nitrides for Photocatalytic and Photoelectrocatalytic Applications. *Mater. Horizons* **2023**, *10* (4), 1363−1372.
(143) Fang, X.; Gao, R.; Yang, Y.; Yan, D. A Cocrystal Precursor Strategy for Carbon-Rich Graphitic Carbon Nitride toward High-Efficiency Photocatalytic Overall Water Splitting. *iScience* **2019**, *16*, 22−30.
(144) Jiang, Y.; Lin, Z.; Zhang, Y.; Lai, Y.; Liang, D.; Yang, C. Facile Synthesis of Porous C-Doped C_3N_4: Fast Charge Separation and Enhanced Photocatalytic Hydrogen Evolution. *New J. Chem.* **2020**, *44* (41), 17891−17898.
(145) Wei, F.; Liu, Y.; Zhao, H.; Ren, X.; Liu, J.; Hasan, T.; Chen, L.; Li, Y.; Su, B.-L. Oxygen Self-Doped g-C_3N_4 with Tunable Electronic Band Structure for Unprecedentedly Enhanced Photocatalytic Performance. *Nanoscale* **2018**, *10* (9), 4515−4522.
(146) Fu, J.; Zhu, B.; Jiang, C.; Cheng, B.; You, W.; Yu, J. Hierarchical Porous O-Doped g-C_3N_4 with Enhanced Photocatalytic CO_2 Reduction Activity. *Small* **2017**, *13* (15), No. 1603938.
(147) Li, H.; Zhang, Z.; Liu, Y.; Cen, W.; Luo, X. Functional Group Effects on the HOMO−LUMO Gap of g-C_3N_4. *Nanomaterials* **2018**, *8* (8), 589.
(148) Shi, W.; Cao, L.; Shi, Y.; Chen, Z.; Cai, Y.; Guo, F.; Du, X. Environmentally Friendly Supermolecule Self-Assembly Preparation of S-Doped Hollow Porous Tubular g-C_3N_4 for Boosted Photocatalytic H_2 Production. *Ceram. Int.* **2023**, *49* (8), 11989−11998.
(149) Yang, H.; Zhou, Y.; Wang, Y.; Hu, S.; Wang, B.; Liao, Q.; Li, H.; Bao, J.; Ge, G.; Jia, S. Three-Dimensional Flower-like Phosphorus-Doped g-C_3N_4 with a High Surface Area for Visible-Light Photocatalytic Hydrogen Evolution. *J. Mater. Chem. A* **2018**, *6* (34), 16485−16494.
(150) Chen, P.; Xing, P.; Chen, Z.; Lin, H.; He, Y. Rapid and Energy-Efficient Preparation of Boron Doped g-C_3N_4 with Excellent Performance in Photocatalytic H_2-Evolution. *Int. J. Hydrogen Energy* **2018**, *43* (43), 19984−19989.
(151) Lan, Z.-A.; Zhang, G.; Wang, X. A Facile Synthesis of Br-Modified g-C_3N_4 Semiconductors for Photoredox Water Splitting. *Appl. Catal. B Environ.* **2016**, *192*, 116−125.
(152) Zhang, G.; Zhang, M.; Ye, X.; Qiu, X.; Lin, S.; Wang, X. Iodine Modified Carbon Nitride Semiconductors as Visible Light Photocatalysts for Hydrogen Evolution. *Adv. Mater.* **2014**, *26* (5), 805−809.
(153) Liu, X.; Yan, L.; Hu, X.; Feng, H.; Guo, B.; Ha, X.; Xu, H. Facile Synthesis of B and P Doped g-C_3N_4 for Enhanced Synergetic Activity between Photocatalytic Water Splitting and BPA Degradation. *Int. J. Hydrogen Energy* **2023**, *48* (35), 13181−13188.
(154) Chuang, P.-K.; Wu, K.-H.; Yeh, T.-F.; Teng, H. Extending the π-Conjugation of g-C_3N_4 by Incorporating Aromatic Carbon for Photocatalytic H_2 Evolution from Aqueous Solution. *ACS Sustain. Chem. Eng.* **2016**, *4* (11), 5989−5997.
(155) Yang, C.; Zhang, S.; Huang, Y.; Lv, K.; Fang, S.; Wu, X.; Li, Q.; Fan, J. Sharply Increasing the Visible Photoreactivity of g-C_3N_4 by Breaking the Intralayered Hydrogen Bonds. *Appl. Surf. Sci.* **2020**, *505*, No. 144654.
(156) Guo, Q.; Zhang, Y.; Qiu, J.; Dong, G. Engineering the Electronic Structure and Optical Properties of g-C_3N_4 by Non-Metal Ion Doping. *J. Mater. Chem. C* **2016**, *4* (28), 6839−6847.
(157) Gao, Y.; Li, Y.; Shangguan, L.; Mou, Z.; Zhang, H.; Ge, D.; Sun, J.; Xia, F.; Lei, W. Optimizing the Band Structure of Sponge-like S-Doped Poly(Heptazine Imide) with Quantum Confinement Effect towards Boosting Visible-Light Photocatalytic H_2 Generation. *J. Colloid Interface Sci.* **2023**, *644*, 116−123.
(158) Wang, J.; Jiang, Z. Ultrasonic-Assisted Synthesis of Porous S-Doped Carbon Nitride Ribbons for Photocatalytic Reduction of CO_2. *Ultrason. Sonochem.* **2023**, *92*, No. 106273.
(159) Zhang, H.; Tang, Y.; Liu, Z.; Zhu, Z.; Tang, X.; Wang, Y. Study on Optical Properties of Alkali Metal Doped g-C_3N_4 and Their Photocatalytic Activity for Reduction of CO_2. *Chem. Phys. Lett.* **2020**, *751*, No. 137467.
(160) Wang, W.; Shu, Z.; Zhou, J.; Meng, D.; Zhao, Z.; Li, T. Facile Synthesis and Microstructure Modulation of Crystalline Polymeric

https://doi.org/10.1021/acsanm.3c04740
ACS Appl. Nano Mater. 2023, 6, 19551−19572

Carbon Nitride for Highly Boosted Photocatalytic Hydrogen Evolution. *J. Mater. Chem. A* **2020**, *8* (14), 6785−6794.
(161) Wang, W.; Xu, P.; Chen, M.; Zeng, G.; Zhang, C.; Zhou, C.; Yang, Y.; Huang, D.; Lai, C.; Cheng, M.; Hu, L.; Xiong, W.; Guo, H.; Zhou, M. Alkali Metal-Assisted Synthesis of Graphite Carbon Nitride with Tunable Band-Gap for Enhanced Visible-Light-Driven Photocatalytic Performance. *ACS Sustain. Chem. Eng.* **2018**, *6* (11), 15503−15516.
(162) Yan, W.; Yan, L.; Jing, C. Impact of Doped Metals on Urea-Derived g-C_3N_4 for Photocatalytic Degradation of Antibiotics: Structure, Photoactivity and Degradation Mechanisms. *Appl. Catal. B Environ.* **2019**, *244*, 475−485.
(163) Xiao, X.; Gao, Y.; Zhang, L.; Zhang, J.; Zhang, Q.; Li, Q.; Bao, H.; Zhou, J.; Miao, S.; Chen, N.; Wang, J.; Jiang, B.; Tian, C.; Fu, H. A Promoted Charge Separation/Transfer System from Cu Single Atoms and C_3N_4 Layers for Efficient Photocatalysis. *Adv. Mater.* **2020**, *32* (33), No. 2003082.
(164) Luo, J.; Han, H.; Wang, X.; Lai, Y.; Liu, B.; Zhong, R.; Zhang, Y.; Zhang, S.; Wang, L. Constructing Oxygen Absorption and Activation Sites in Ce-Doped g-C_3N_4 Photocatalyst for Effective Removal of Amoxicillin: Performance, Mechanism and Degradation Pathways. *Appl. Surf. Sci.* **2023**, *611*, No. 155808.
(165) Ismael, M. One-Step Ultrasonic-Assisted Synthesis of Ni-Doped g-C_3N_4 Photocatalyst for Enhanced Photocatalytic Hydrogen Evolution. *Inorg. Chem. Commun.* **2023**, *151*, No. 110607.
(166) Deng, P.; Xiong, J.; Lei, S.; Wang, W.; Ou, X.; Xu, Y.; Xiao, Y.; Cheng, B. Nickel Formate Induced High-Level in Situ Ni-Doping of g-C_3N_4 for a Tunable Band Structure and Enhanced Photocatalytic Performance. *J. Mater. Chem. A* **2019**, *7* (39), 22385−22397.
(167) Yue, B.; Li, Q.; Iwai, H.; Kako, T.; Ye, J. Hydrogen Production Using Zinc-Doped Carbon Nitride Catalyst Irradiated with Visible Light. *Sci. Technol. Adv. Mater.* **2011**, *12* (3), No. 034401.
(168) Hu, S.; Jin, R.; Lu, G.; Liu, D.; Gui, J. The Properties and Photocatalytic Performance Comparison of Fe^{3+}-Doped g-C_3N_4 and Fe_2O_3/g-C_3N_4 Composite Catalysts. *RSC Adv.* **2014**, *4* (47), 24863.
(169) Gao, J.; Wang, Y.; Zhou, S.; Lin, W.; Kong, Y. A Facile One-Step Synthesis of Fe-Doped g-C_3N_4 Nanosheets and Their Improved Visible-Light Photocatalytic Performance. *ChemCatChem.* **2017**, *9* (9), 1708−1715.
(170) Li, Y.; Wang, Z.; Xia, T.; Ju, H.; Zhang, K.; Long, R.; Xu, Q.; Wang, C.; Song, L.; Zhu, J.; Jiang, J.; Xiong, Y. Implementing Metal-to-Ligand Charge Transfer in Organic Semiconductor for Improved Visible-Near-Infrared Photocatalysis. *Adv. Mater.* **2016**, *28* (32), 6959−6965.
(171) Wang, N.; Wang, J.; Hu, J.; Lu, X.; Sun, J.; Shi, F.; Liu, Z.-H.; Lei, Z.; Jiang, R. Design of Palladium-Doped g-C_3N_4 for Enhanced Photocatalytic Activity toward Hydrogen Evolution Reaction. *ACS Appl. Energy Mater.* **2018**, *1* (6), 2866−2873.
(172) Chen, P.-W.; Li, K.; Yu, Y.-X.; Zhang, W.-D. Cobalt-Doped Graphitic Carbon Nitride Photocatalysts with High Activity for Hydrogen Evolution. *Appl. Surf. Sci.* **2017**, *392*, 608−615.
(173) Zhang, M.; Bai, X.; Liu, D.; Wang, J.; Zhu, Y. Enhanced Catalytic Activity of Potassium-Doped Graphitic Carbon Nitride Induced by Lower Valence Position. *Appl. Catal. B Environ.* **2015**, *164*, 77−81.
(174) Zhang, J.; Hu, S.; Wang, Y. A Convenient Method to Prepare a Novel Alkali Metal Sodium Doped Carbon Nitride Photocatalyst with a Tunable Band Structure. *RSC Adv.* **2014**, *4* (108), 62912−62919.
(175) Jin, R.; Hu, S.; Gui, J.; Liu, D. A Convenient Method to Prepare Novel Rare Earth Metal Ce-Doped Carbon Nitride with Enhanced Photocatalytic Activity Under Visible Light. *Bull. Korean Chem. Soc.* **2015**, *36* (1), 17−23.
(176) Li, Y.; Lai, C.; Zhong, J.; Li, J. Largely Elevated Photocatalytic Hydrogen Generation over Eu Doped g-C_3N_4 Photocatalyst. *Int. J. Hydrogen Energy* **2023**, *48* (63), 24356−24368.
(177) Yang, X.; Guo, Z.; Zhang, X.; Han, Y.; Xue, Z.; Xie, T.; Yang, W. The Effect of Indium Doping on the Hydrogen Evolution Performance of g-C_3N_4 Based Photocatalysts. *New J. Chem.* **2021**, *45* (2), 544−550.
(178) Wang, Y.; Li, Y.; Bai, X.; Cai, Q.; Liu, C.; Zuo, Y.; Kang, S.; Cui, L. Facile Synthesis of Y-Doped Graphitic Carbon Nitride with Enhanced Photocatalytic Performance. *Catal. Commun.* **2016**, *84*, 179−182.
(179) Tasleem, S.; Tahir, M. Synergistically Improved Charge Separation in Bimetallic Co−La Modified 3D g-C_3N_4 for Enhanced Photocatalytic H_2 Production under UV−Visible Light. *Int. J. Hydrogen Energy* **2021**, *46* (40), 20995−21012.
(180) Kumar, P.; Vahidzadeh, E.; Thakur, U. K.; Kar, P.; Alam, K. M.; Goswami, A.; Mahdi, N.; Cui, K.; Bernard, G. M.; Michaelis, V. K.; Shankar, K. C_3N_5: A Low Bandgap Semiconductor Containing an Azo-Linked Carbon Nitride Framework for Photocatalytic, Photovoltaic and Adsorbent Applications. *J. Am. Chem. Soc.* **2019**, *141* (13), 5415−5436.
(181) Mane, G. P.; Talapaneni, S. N.; Lakhi, K. S.; Ilbeygi, H.; Ravon, U.; Al-Bahily, K.; Mori, T.; Park, D.; Vinu, A. Highly Ordered Nitrogen-Rich Mesoporous Carbon Nitrides and Their Superior Performance for Sensing and Photocatalytic Hydrogen Generation. *Angew. Chemie Int. Ed.* **2017**, *56* (29), 8481−8485.
(182) Mahmood, J.; Lee, E. K.; Jung, M.; Shin, D.; Jeon, I.-Y.; Jung, S.-M.; Choi, H.-J.; Seo, J.-M.; Bae, S.-Y.; Sohn, S.-D.; Park, N.; Oh, J. H.; Shin, H.-J.; Baek, J.-B. Nitrogenated Holey Two-Dimensional Structures. *Nat. Commun.* **2015**, *6* (1), 6486.
(183) Godin, R.; Wang, Y.; Zwijnenburg, M. A.; Tang, J.; Durrant, J. R. Time-Resolved Spectroscopic Investigation of Charge Trapping in Carbon Nitrides Photocatalysts for Hydrogen Generation. *J. Am. Chem. Soc.* **2017**, *139* (14), 5216−5224.
(184) Corp, K. L.; Schlenker, C. W. Ultrafast Spectroscopy Reveals Electron-Transfer Cascade That Improves Hydrogen Evolution with Carbon Nitride Photocatalysts. *J. Am. Chem. Soc.* **2017**, *139* (23), 7904−7912.
(185) Yang, W.; Godin, R.; Kasap, H.; Moss, B.; Dong, Y.; Hillman, S. A. J.; Steier, L.; Reisner, E.; Durrant, J. R. Electron Accumulation Induces Efficiency Bottleneck for Hydrogen Production in Carbon Nitride Photocatalysts. *J. Am. Chem. Soc.* **2019**, *141* (28), 11219−11229.
(186) Tong, X.; Shou, J.; Song, H.; Wang, Y.; Huang, L.; Yin, L. Ultrafast Electron Transfer from Crystalline g-C_3N_4 to Pt Revealed by Femtosecond Transient Absorption Spectroscopy. *Energy Fuels* **2022**, *36* (19), 11532−11541.
(187) Lin, Q.; Li, Z.; Lin, T.; Li, B.; Liao, X.; Yu, H.; Yu, C. Controlled Preparation of P-Doped g-C_3N_4 Nanosheets for Efficient Photocatalytic Hydrogen Production. *Chin. J. Chem. Eng.* **2020**, *28* (10), 2677−2688.
(188) Zhao, Z.; Xie, C.; Cui, H.; Wang, Q.; Shu, Z.; Zhou, J.; Li, T. Scalable One-Pot Synthesis of Phosphorus-Doped g-C_3N_4 Nanosheets for Enhanced Visible-Light Photocatalytic Hydrogen Evolution. *Diam. Relat. Mater.* **2020**, *104*, No. 107734.
(189) Wang, J.; Cui, W.; Chen, R.; He, Y.; Yuan, C.; Sheng, J.; Li, J.; Zhang, Y.; Dong, F.; Sun, Y. OH/Na Co-Functionalized Carbon Nitride: Directional Charge Transfer and Enhanced Photocatalytic Oxidation Ability. *Catal. Sci. Technol.* **2020**, *10* (2), 529−535.
(190) Li, H.-J.; Sun, B.-W.; Sui, L.; Qian, D.-J.; Chen, M. Preparation of Water-Dispersible Porous g-C_3N_4 with Improved Photocatalytic Activity by Chemical Oxidation. *Phys. Chem. Chem. Phys.* **2015**, *17* (5), 3309−3315.
(191) Teng, Z.; Yang, N.; Lv, H.; Wang, S.; Hu, M.; Wang, C.; Wang, D.; Wang, G. Edge-Functionalized g-C_3N_4 Nanosheets as a Highly Efficient Metal-Free Photocatalyst for Safe Drinking Water. *Chem.* **2019**, *5* (3), 664−680.
(192) Safaei, J.; Mohamed, N. A.; Noh, M. F. M.; Soh, M. F.; Riza, M. A.; Mustakim, N. S. M.; Ludin, N. A.; Ibrahim, M. A.; Isahak, W. N. R. W.; Teridi, M. A. M. Facile Fabrication of Graphitic Carbon Nitride, (g-C_3N_4) Thin Film. *J. Alloys Compd.* **2018**, *769*, 130−135.
(193) Xiong, W.; Huang, F.; Zhang, R.-Q. Recent Developments in Carbon Nitride Based Films for Photoelectrochemical Water Splitting. *Sustain. Energy Fuels* **2020**, *4* (2), 485−503.

https://doi.org/10.1021/acsanm.3c04740
ACS Appl. Nano Mater. 2023, 6, 19551−19572

(194) Minegishi, T.; Nishimura, N.; Kubota, J.; Domen, K. Photoelectrochemical Properties of $LaTiO_2N$ Electrodes Prepared by Particle Transfer for Sunlight-Driven Water Splitting. *Chem. Sci.* **2013**, *4* (3), 1120.
(195) Ham, Y.; Minegishi, T.; Hisatomi, T.; Domen, K. A $SrTiO_3$ Photoanode Prepared by the Particle Transfer Method for Oxygen Evolution from Water with High Quantum Efficiencies. *Chem. Commun.* **2016**, *52* (28), 5011−5014.
(196) Liu, J.; Hisatomi, T.; Ma, G.; Iwanaga, A.; Minegishi, T.; Moriya, Y.; Katayama, M.; Kubota, J.; Domen, K. Improving the Photoelectrochemical Activity of $La_5Ti_2CuS_5O_7$ for Hydrogen Evolution by Particle Transfer and Doping. *Energy Environ. Sci.* **2014**, *7* (7), 2239−2242.
(197) Kumagai, H.; Minegishi, T.; Moriya, Y.; Kubota, J.; Domen, K. Photoelectrochemical Hydrogen Evolution from Water Using Copper Gallium Selenide Electrodes Prepared by a Particle Transfer Method. *J. Phys. Chem. C* **2014**, *118* (30), 16386−16392.

https://doi.org/10.1021/acsanm.3c04740
ACS Appl. Nano Mater. 2023, 6, 19551−19572